



Review

# Recent Advances on Ultrasound Contrast Agents for Blood-Brain Barrier Opening with Focused Ultrasound

Ambre Dauba <sup>1</sup>, Anthony Delalande <sup>2</sup>, Hermes A. S. Kamimura <sup>3</sup>, Allegra Conti <sup>4</sup>, Benoit Larrat <sup>5</sup>, Nicolas Tsapis <sup>6</sup> and Anthony Novell <sup>1,\*</sup>

<sup>1</sup> Université Paris-Saclay, CEA, CNRS, Inserm, BioMaps, Service Hospitalier Frédéric Joliot, 91401 Orsay, France; ambre.dauba@universite-paris-saclay.fr

<sup>2</sup> Centre de Biophysique Moléculaire and Université d'Orléans, CNRS-UPR 4301, 45071 Orléans, France; anthony.delalande@cnrs.fr

<sup>3</sup> Department of Biomedical Engineering, Columbia University, New York, NY 10032, USA; kamimura.hermes@columbia.edu

<sup>4</sup> Department of Biomedicine and Prevention, University of Rome Tor Vergata, 00133 Rome, Italy; allegra.conti@uniroma2.it

<sup>5</sup> Université Paris-Saclay, CEA, CNRS, Baobab, NeuroSpin, 91191 Gif-sur-Yvette, France; benoit.larrat@cea.fr

<sup>6</sup> Université Paris-Saclay, CNRS, Institut Galien Paris-Saclay, 92296 Châtenay-Malabry, France; nicolas.tsapis@universite-paris-saclay.fr

\* Correspondence: anthony.novell@universite-paris-saclay.fr; Tel.: +33-169867727

Received: 19 October 2020; Accepted: 17 November 2020; Published: 21 November 2020



**Abstract:** The blood-brain barrier is the primary obstacle to efficient intracerebral drug delivery. Focused ultrasound, in conjunction with microbubbles, is a targeted and non-invasive way to disrupt the blood-brain barrier. Many commercially available ultrasound contrast agents and agents specifically designed for therapeutic purposes have been investigated in ultrasound-mediated blood-brain barrier opening studies. The new generation of sono-sensitive agents, such as liquid-core droplets, can also potentially disrupt the blood-brain barrier after their ultrasound-induced vaporization. In this review, we describe the different compositions of agents used for ultrasound-mediated blood-brain barrier opening in recent studies, and we discuss the challenges of the past five years related to the optimal formulation of agents.

**Keywords:** blood-brain barrier; bubble; droplet; phase-change contrast agent; ultrasound

## 1. Introduction

The brain homeostasis is maintained by the blood-brain barrier (BBB), composed of tight junctions between endothelial cells on the vessel walls. The BBB, while preventing the entry of potentially harmful compounds, is the primary obstacle to efficient intracerebral delivery of almost all pharmaceuticals developed to treat neurological diseases, especially large molecule compounds [1]. Of the several techniques to deliver drugs across the BBB [1], the use of focused ultrasound (FUS) in conjunction with microbubbles is of great interest as it is targeted, transient, non-invasive, and safe [2]. This effectiveness of this technique was demonstrated for the first time by Hynynen et al. in 2001 [3]. After a few hours, gradual closure of the BBB and normal functioning was observed [1,4,5]. The safety has also been demonstrated in small animals and in non-human primates through histological evaluation and behavioral studies after FUS-mediated BBB disruption at multiple times and locations [6,7]. More recently, phase I and II clinical trials have shown the safety of this technique in humans [8].

This evidence strongly supports that, using suitable parameters, FUS is safe for BBB opening with a great potential to treat many brain diseases.

FUS-induced BBB opening enhances the delivery of drugs in the central nervous system [9–11]. Currently, the FUS-induced delivery of several compounds is under investigation for the treatment of diseases such as glioblastoma [12], neurodegenerative diseases like Alzheimer's [13], Parkinson's [14], or genetic diseases [15]. Additionally, FUS combined with microbubbles can achieve therapeutic results alone: it can induce, for example, neurogenesis [16] or reduce the amyloid load in Alzheimer's disease [17]. The approach is usually combined with magnetic resonance imaging (MRI), which enables the treatment guidance, the evaluation of BBB disruption using MR contrast agents, and the monitoring of potential damages during the procedure [3,18–22].

The addition of microbubbles has reduced the amount of ultrasound energy required to open the BBB by 100-fold [2,3]. Upon sonication, microbubbles start oscillating at the frequency of ultrasound. Above a certain acoustic pressure, the previously symmetrical oscillations of the bubble become unstable [23]. Those two different regimens are respectively called stable and inertial cavitation. Inertial cavitation can induce microbubble collapse accompanied by micro-jetting, fragmentation, and shock-wave formation, which may induce vascular endothelium damages [20,22,24,25]. On the other hand, the mechanical stress generated by the stable cavitation can locally and reversibly disrupt the tight junctions present in the vascular endothelial tissue, which increases the BBB permeability [26]. It is generally accepted that stable cavitation is the preferred regime for a safe BBB opening [26]. Figure 1 schematically presents the two oscillation regimens of microbubbles and their potential effects on BBB. The use of low acoustic pressure (few hundreds of kPa) ensures the safety of the technique by limiting any potential damages such as erythrocyte extravasation, hemorrhage, and necrotic damage [27] resulting from local thermal [28] or mechanical effects [24,27].

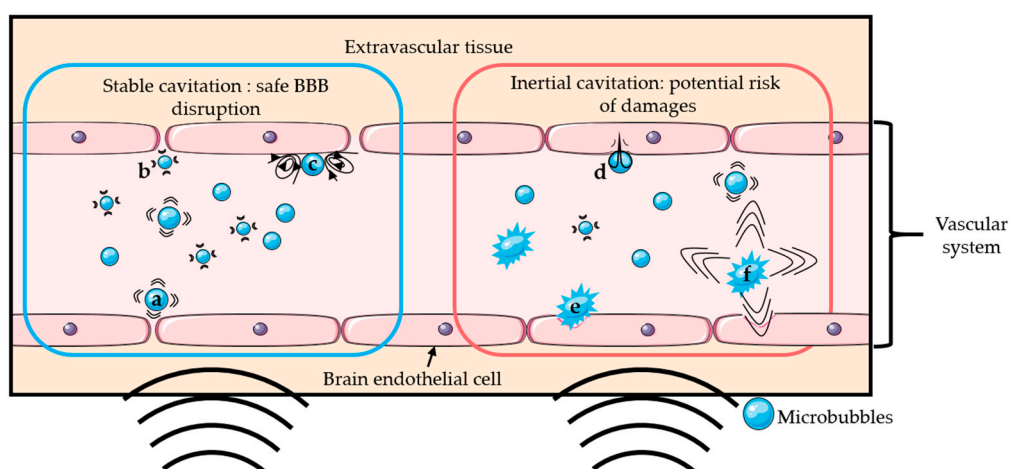


**Figure 1.** Schematic representation of several mechanisms of BBB disruption: Stable cavitation induces push- (a) and pull (b) mechanism and microstreaming (c), which can permeabilize the blood-brain barrier safely. Inertial cavitation induces micro-jetting (d), fragmentation (e), and shock-wave (f) that can permeabilize the BBB with risks of damages.

Microbubbles consist of a gas core coated/encapsulated by a stabilizing shell. The coating provides a gas diffusion barrier while the gas core, composed of a heavy molecular weight inert gas, improves the bubble half-life after injection thanks to its low solubility in the surrounding medium [29,30]. Figure 2 shows a typical microscopic picture of polydisperse lipid-shelled microbubbles and their size distribution. The typical size of a microbubble is between 1 and 10  $\mu\text{m}$  in diameter [29]. Sub-micronic bubbles (between 100 nm and 1  $\mu\text{m}$ ) are usually named nanobubbles in the literature. In order to be used for BBB opening, bubbles have to be (i) compressible to undergo cavitation, (ii) stable to circulate

long enough to fulfill their duty, and (iii) non-toxic. After injection into the bloodstream, microbubbles circulate for only a few minutes before being cleared [31].

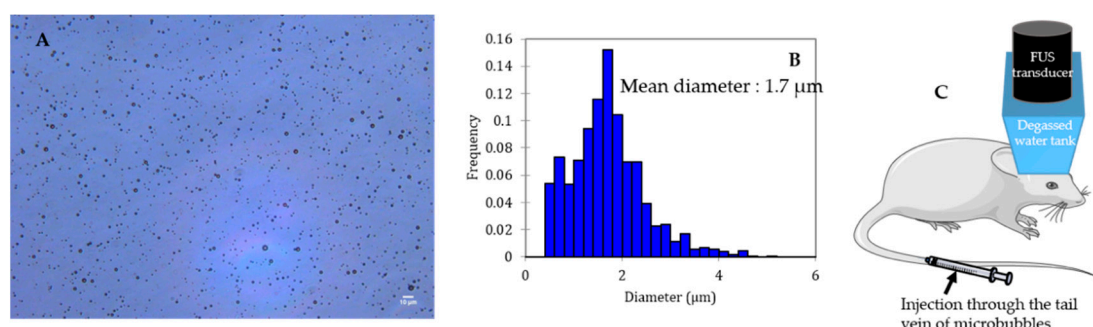


**Figure 2.** Size distribution characterization of a lipid shelled microbubble solution. Shell composition: 1,2-distearoyl-sn-glycero-3-phosphocholine (DSPC) 9:1 1,2-dimyristoyl-sn-glycero-3-phosphoethanolamine -N-[methoxy(polyethylene glycol)-2000] (DSPE-PEG2000). Core composition: decafluorobutane. (A) Microscopic picture of the solution (dilution: 1:10; scale: 10  $\mu\text{m}$ ), (B) size distribution of the solution, (C) schematic representation of BBB opening on mice.

Ultrasound contrast agents (UCAs) initially designed as echogenic contrast agents and clinically approved for diagnostic applications have also been shown capable of disrupting the BBB. However, bubbles can be formulated specifically for BBB disruption. Additionally, UCAs can be loaded with MRI contrast agent molecules, which allows imaging of their biodistribution. Targeting ligands can be added to the UCAs surface to increase their specificity or engineered with embedded drugs for targeted release, which reduces systemic drug effects.

An ultrasound can be used to convert droplets, called emulsions or phase-change contrast agents (PCCA), into microbubbles. For this reason, a droplet can also be designed for BBB opening. In vivo, a sufficient peak rarefactional pressure is necessary to vaporize the droplet's liquid core [32]. Acoustic droplet vaporization (ADV) and the cavitation of the resulting bubble can induce BBB opening [33].

A systematic review of the recent literature was performed to build a database of the different materials employed for the shell and core of agents used to open the BBB with FUS. A discussion about the different possibilities to find the right balance between reaching a stable cavitation regimen and agent stability is presented. Following that, we present a summary of the different multifunctional agents used to disrupt the BBB with FUS, enhance MRI contrast, or molecularly target a specific area of the brain or/and carry drug all at once. We finish the review with a description of the latest developments on engineered biomolecules, which open new avenues for cell-based therapy and diagnostic. To the best of our knowledge, this is the first review to provide a database of the different materials recently used to disrupt the BBB transiently with FUS.

## 2. Recent Advances on Sono-Sensitive Agents for Ultrasound-Assisted Blood-Brain Barrier Opening

### 2.1. Method of Literature Search

We searched on PubMed in October 2020 for all studies on BBB disruption induced by FUS in conjunction with microbubbles or nanodroplets using search terms (microbubble OR nanodroplet OR nanoemulsion OR “phase-change contrast agent”) AND (“blood-brain barrier” OR “brain-targeted drug delivery”) AND (ultrasound). We limited the search to the last 5 years (from 7 May 2015 to 1 October 2020), which yielded 247 studies. After screening titles and abstracts, we only kept articles that studied FUS-induced BBB opening in vivo as a therapeutic purpose. We thus excluded studies about BBB inflammatory response, passive acoustic mapping, and computer simulation. We also excluded studies that did not provide enough information about the agent used to disrupt the BBB.

As a result, 105 studies were included for data extraction and synthesis. The selection included 6 clinical trials, 8 preclinical studies on large animals, and 91 on small animals (rodents and rabbits). 53 studies used commercially available contrast agents, and 55 studies described agents explicitly designed for BBB opening purpose. Three of these studies compared commercial and self-made contrast agents. Among these studies, 54 used MRI to assess and/or guide BBB opening. The flow diagram of the search is presented in Figure 3.

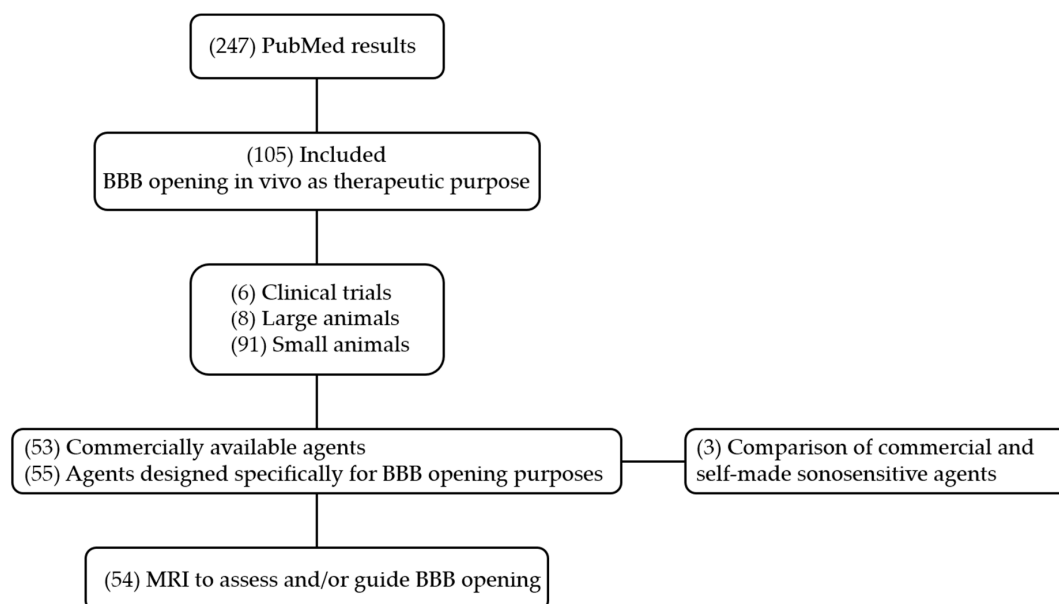


**Figure 3.** Flow chart of PubMed.

This search has brought to our attention several reviews that supplement the present one [31,34]. In addition, an overview of other strategies for brain drug delivery can be found in [35].

## 2.2. Commercial Ultrasound Contrast Agents

Commercially available UCAs used for BBB opening are either clinically approved as imaging contrast agents (Food and Drug Administration or European Medicines Agency) or are being developed specifically for therapeutic purposes. The clinically approved microbubbles used to disrupt the BBB with FUS are Definity™ (Lantheus Medical Imaging, North Billerica, MA, USA), SonoVue®/Lumason® (Bracco, Milan, Italy), Optison™ (GE Healthcare, Milwaukee, WI, USA), and Sonazoid® (GE Healthcare, Milwaukee, WI, USA). Other commercially available UCAs resulted in successful BBB opening such as USphere® (Trust Bio-sonics, Zhubei City, Taiwan), SIMB® (Advanced Microbubbles Inc, Boulder, CO, USA), Vevo MicroMarker® (Fujifilm, Toronto, ON, Canada), BR-38® and others (Bracco Suisse SA, Geneva, Switzerland), and bubbles ordered from Targeson Inc. (San Diego, CA, USA). These agents consist of lipid or protein shells with gaseous sulfur hexafluoride (SF<sub>6</sub>) or perfluorocarbon (PFC) cores. Table 1 summarizes the commercial and non-commercial UCAs used to disrupt the BBB with ultrasounds in pre-clinical studies during the past 5 years, their composition, and associated references.

**Table 1.** Composition and phase of sono-sensitive agents used for BBB opening over the past 5 years.

Commercial Name	Phase	Core	Shell	References
Definity (Lantheus Medical Imaging)	gas	C <sub>3</sub> F <sub>8</sub>	lipid	[12,13,16,36–53]
SonoVue/Lumason (Bracco)	gas	SF <sub>6</sub>	lipid	[15,36,37,54–68]
Optison (GE Healthcare)	gas	C <sub>3</sub> F <sub>8</sub>	protein	[38,69–74]
SIMB (Advanced Microbubbles Inc)	gas	“gas”	lipid	[75]
Vevo MicroMarker (Fujifilm)	gas	C <sub>4</sub> F <sub>10</sub> and N <sub>2</sub>	lipid	[76]
BG8235 similar to BR-38 (Bracco)	gas	C <sub>4</sub> F <sub>10</sub>	lipid	[77]
Targeson Inc	gas	PFC	lipid	[78]
USphere (Trust Bio-sonics)	gas	C <sub>3</sub> F <sub>8</sub>	lipid	[37]
Sonazoid (GE Healthcare)	gas	C <sub>4</sub> F <sub>10</sub>	lipid	[68]
Sonazoid (GE Healthcare)	AC: gas and liquid	Sonazoid bubbles: C <sub>4</sub> F <sub>10</sub> Homemade droplets: C <sub>6</sub> F <sub>12</sub>	lipid	[79]
Non-commercial	liquid	C <sub>3</sub> F <sub>8</sub> or C <sub>4</sub> F <sub>10</sub>	lipid	[33]
Non-commercial	liquid	C <sub>5</sub> F <sub>12</sub>	lipid	[80]
Non-commercial	gas	C <sub>3</sub> F <sub>8</sub>	protein	[81–83]
Non-commercial	gas	C <sub>3</sub> F <sub>8</sub>	self-assembled polymeric nanoparticles	[84]
Non-commercial	gas	C <sub>3</sub> F <sub>8</sub>	self-assembled polymeric nanoparticles and protein	[85]
Non-commercial	gas	air	polymer	[86,87]
Non-commercial	gas	C <sub>5</sub> F <sub>12</sub>	polymer	[88]
Non-commercial	gas	SF <sub>6</sub>	lipid	[68,89,90]
Non-commercial	gas	C <sub>4</sub> F <sub>10</sub>	lipid	[6,11,14,39,68,91–103]
Non-commercial	gas	C <sub>3</sub> F <sub>8</sub>	lipid	[38,68,104–126]

AC: Acoustic cluster; PFC: perfluorocarbon; C<sub>3</sub>F<sub>8</sub>: octafluoropropane; C<sub>4</sub>F<sub>10</sub>: decafluorobutane; C<sub>5</sub>F<sub>12</sub>: dodecafluoropentane; C<sub>6</sub>F<sub>12</sub>: perfluoromethylcyclopentane; SF<sub>6</sub>: sulphur hexafluoride; N<sub>2</sub>: nitrogen.

We came across four studies comparing different commercially available bubbles on their abilities to open the BBB by assessing Evans blue leakage in the brain (commonly used dye for BBB permeability assessment, otherwise blocked by the BBB). The obtained results for these 4 studies are summarized in Table 2, along with the bubble type, injection dose, and ultrasonic parameters used for the BBB disruption. Briefly, Shin et al. compared a dose of SonoVue at 30 µL/kg with two different doses of Definity at 20 µL/kg and 100 µL/kg. Definity microbubbles at a 20 µL/kg dose were more effective for BBB opening and led to fewer damages than SonoVue. For the 100 µL/kg dose of Definity, the BBB opening was more important, and the level of tissue damages (histological evaluation) was similar to SonoVue microbubbles at 30 µL/kg [36]. Wu et al. compared SonoVue, Definity, and USphere at an injected microbubble concentration of  $4 \times 10^7$  bubbles/kg. For a given set of sonication parameters, the order of Evans blue penetration (from the most important to the weakest) was: SonoVue, Definity, USphere [37]. Bing et al. compared Optison and Definity performances. The concentration of bubbles was adjusted to inject the same gas volume (1.1–1.2 µL/mL). Evans blue leakage was more important for Optison microbubbles than for Definity [38]. Finally, Omata et al. compared SonoVue and Sonazoid at an injected microbubble concentration of  $3 \times 10^9$  bubbles/kg and showed a higher Evans blue leakage with the Sonazoid bubbles [68].

In the Wu et al. study, a 200 µL/kg dose of SonoVue microbubbles successfully opened the BBB without damages using a higher peak negative pressure and a more prolonged exposure than the Shin et al. study where damages on the rat brain were observed for a 20 µL/kg dose of SonoVue. This inconsistency between the two studies points out that the BBB opening effectiveness and safety should be studied in-depth, ideally comparing different commercially available bubbles. Omata et al. showed that a 30,000 µL/kg dose of SonoVue successfully opened the mice BBB without damages. However, the comparison with Wu et al. and Shin et al. is trickier as they studied mice for which the skull is thinner than rats. Furthermore, ultrasound parameters such as the frequency used (3 MHz) for BBB opening differs from other studies making the comparison challenging. As another example, the Wu et al. study demonstrates a higher efficacy of SonoVue over Definity while the Shin et al. study

tends to the opposite direction. Importantly, injected doses play a critical role. Besides, commercially available agents explicitly made for BBB opening purposes would be desirable.

**Table 2.** Comparison of different commercial bubbles regarding BBB opening.

Ref	Bubble Type	Injection Dose ( $\mu\text{L}/\text{kg}$ )	Number of Bubbles per mL	Animal	Acoustic Parameters	Evans Blue Leakage	Damages Score
Bing et al. [38]	Optison	30	$7 \times 10^8$	Sprague Dawley rats (230–300 g)	PnP = 0.47 MPa $f_c$ = 0.75 MHz PRF = 1 Hz duration = 120 s burst = 10 s	High	NA
	Definity	6	$1 \times 10^{10}$		PnP = 0.3 MPa $f_c$ = 0.5 MHz PRF = 2 Hz duration = 60 s burst = 10 s	Moderate	NA
Shin et al. [36]	SonoVue	30	$2 \times 10^8$	Sprague Dawley rats (250–300 g)	PnP = 0.39 MPa $f_c$ = 0.4 MHz PRF = 1 Hz duration = 120 s	4.45%	1
	Definity	20	$1 \times 10^{10}$		Intensity = $0.5 \text{ W}/\text{cm}^2$ $f_c$ = 3 MHz PRF = 10 Hz duration = 180 s burst = 50 s	13.72%	0
	Definity	100	$1 \times 10^{10}$		burst = 10 s	16.35%	1
Wu et al. [37]	SonoVue	200	$2 \times 10^8$	Sprague Dawley rats (250–300 g)	burst = 10 s	$0.79 \pm 0.24 \mu\text{M}$	0
	Definity	4	$1 \times 10^{10}$		burst = 10 s	$0.52 \pm 0.25 \mu\text{M}$	0
	USphere Sonazoid	1.43 3333	$2.8 \times 10^{10}$ $9 \times 10^8$		burst = 10 s	$18 \pm 7 \mu\text{g}/\text{g brain}$	0
Omata et al. [68]	SonoVue	30,000	$1 \times 10^8$	ddY mice (6 week old)	$f_c$ = 3 MHz PRF = 10 Hz duration = 180 s burst = 50 s	$5 \pm 1 \mu\text{g}/\text{g brain}$	0

PnP = Peak negative Pressure;  $f_c$  = central frequency; PRF = Pulse repetition frequency; NA: non-assessed; the damage score grades hemorrhage and tissue damages: grade 0—normal tissue, grade 1—scattered or discontinuous erythrocyte extravasation, grade 2—continuous extravasation or microhemorrhage, grade 3—hemorrhage with necrotic damage or gross hemorrhage [27].

### 2.3. Design of Specific Agents for Blood-Brain Barrier Opening

While clinically-approved contrast agents expedite therapeutic clinical trials, their compositions originally developed for diagnostic imaging can be suboptimal for BBB opening [127]. Moreover, designing specific BBB disruption agents makes possible their use as multifunctional agents for imaging and drug delivery purposes in theranostics.

Agents designed for BBB disruption, like UCAs, have to fulfill several criteria such as (i) easily reachable stable cavitation regimen, (ii) long in vivo circulation stability, and (iii) storage stability. Thereby, bubbles must undergo sufficient oscillations for a relatively low peak rarefactional pressure before reaching inertial cavitation. Stable and inertial cavitation thresholds have to be assessed, meaning that the lowest acoustic pressure required for the bubble to reach these regimens has to be estimated. The vaporization threshold for droplets, namely the magnitude of acoustic pressure required to convert a liquid droplet into a gaseous bubble, also has to be considered [128]. Over the 55 studies describing agents designed for BBB opening procedures, only 15 performed at least one test to assess cavitation thresholds or stability performances (Table 3). These tests are crucial for the success and safety of the experiments [91]. Therefore, they should be performed on a routine basis, especially since those parameters can be incredibly different from an agent to another (acoustic stability on echography images ranging from few seconds [68] to days [88] depending on the bubble). Currently, most of the bubble-based therapeutic ultrasound protocols are limited to a few minutes or require a repeatable injection of fresh UCAs to extend the circulation of microbubbles in the body and increase the procedure's efficiency. For commercial microbubbles, the half-life in the bloodstream is typically lower than 10 min [129], and extending the in vivo circulation of these agents is desirable.

**Table 3.** Stability and cavitation thresholds assessment for sono-sensitive agents for BBB opening; without other specifications, cavitation thresholds are detected with in vitro passive cavitation detection. The storage stability was assessed by taking samples at several times after agent formulation and checking its echographic stability [80], cavitation emissions [108,125], concentration [39], or therapeutic effect [102].

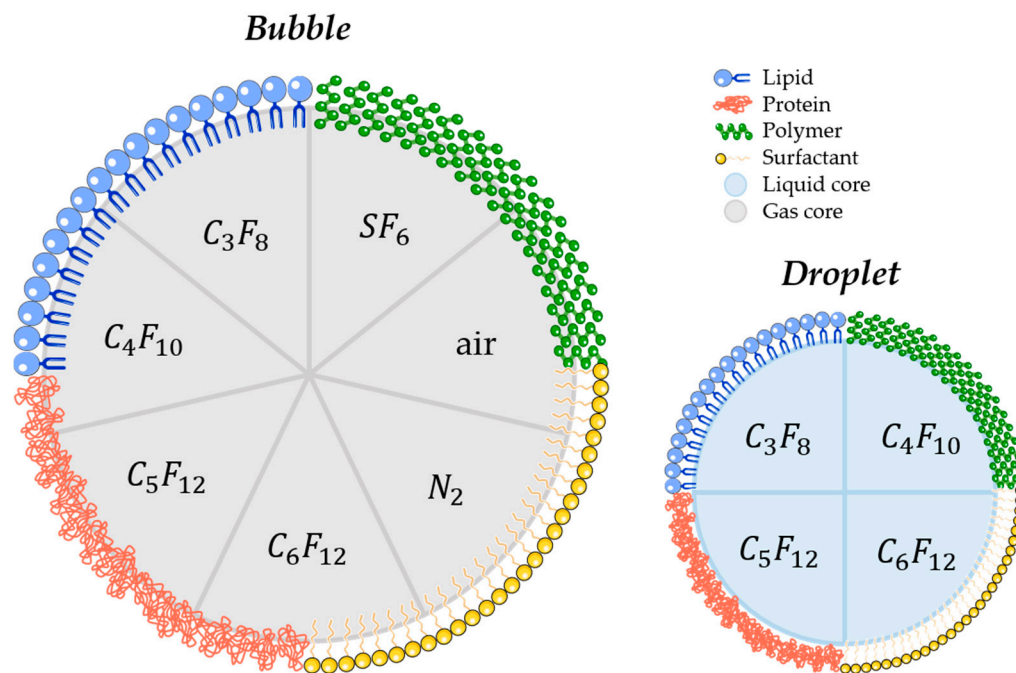
Phase	Core	Shell	Storage Stability	In Vitro Acoustic Stability (Echography)	In Vivo Half-Life	Stable Cavitation Threshold	Inertial Cavitation Threshold	Ref.
liquid	C <sub>5</sub> F <sub>12</sub>	PEG-PLGA	stable 2 days at 4 °C	NA	NA	VT = 1.0 MPa ( <i>f<sub>c</sub></i> = 1 MHz)		[80]
liquid	C <sub>3</sub> F <sub>8</sub> or C <sub>4</sub> F <sub>10</sub>	DSPC: DSPE-PEG2000 (molar ratio 9:1)	NA	NA	NA	C <sub>3</sub> F <sub>8</sub> VT = 0.3 MPa C <sub>4</sub> F <sub>10</sub> VT = 0.75 MPa ( <i>f<sub>c</sub></i> = 1.5 MHz)		[33]
gas	C <sub>3</sub> F <sub>8</sub>	DPPC: DSPE-PEG2000: DPTAP (molar ratio 9:2:1)	NA	relatively stable 50 min at 37 °C	NA	NA	0.3 MPa ( <i>f<sub>c</sub></i> = 1 MHz)	[105]
gas	C <sub>3</sub> F <sub>8</sub>	DPTAP: DPPC: DSPE-PEG2000 (molar ratio 31,5,3,9:1,8)	NA	stable 1 h at 37 °C	10 min (male C57BL/6j mice 20–25 g)	0.3 MPa ( <i>f<sub>c</sub></i> = 1 MHz; BBB opening without damages)	0.5 MPa ( <i>f<sub>c</sub></i> = 1 MHz) 0.175 MPa ( <i>f<sub>c</sub></i> = 0.25 MHz)	[106]
gas	C <sub>3</sub> F <sub>8</sub>	DSPC: DSPE-PEG2000 (molar ratio 9:1)	NA	NA	NA	NA	0.4 MPa ( <i>f<sub>c</sub></i> = 1 MHz)	[91]
gas	C <sub>3</sub> F <sub>8</sub>	DBPC: DPPA: DPPE: DSPE-PEG2000 (molar ratio 6,15,2:1:1)	NA	NA	6–8 min (Sprague Dawley rats 230–300 g)	0.21 MPa in vitro 0.16 MPa in vivo ( <i>f<sub>c</sub></i> = 0.75 MHz)	0.59 MPa in vitro 0.47 MPa in vivo	[38]
gas	C <sub>3</sub> F <sub>8</sub>	DBPC: DPPA: DPPE: DSPE-PEG2000 (molar ratio 6:1:2:1)	stable 2 h at 5 × 10 <sup>10</sup> bubbles/mL	NA	10 min at 10 <sup>11</sup> bubbles/mL (Sprague Dawley rats 230–300 g)	0.31 MPa in vivo ( <i>f<sub>c</sub></i> = 0.75 MHz; 10 <sup>10</sup> bubbles/mL)	0.70 MPa in vivo	[108]
gas	C <sub>3</sub> F <sub>8</sub>	DSPC: DSPE-PEG2000 (molar ratio 9:1)	NA	NA	8 min (nude mice)	NA	NA	[123]
gas	C <sub>3</sub> F <sub>8</sub>	DPPC: DPTAP: DSPE-PEG2000 (molar ratio 31,5,3,9:1,8)	NA	stable 1 h at 37 °C	NA	0.3 MPa ( <i>f<sub>c</sub></i> = 1 MHz)	0.5 MPa ( <i>f<sub>c</sub></i> = 1 MHz)	[107]
gas	C <sub>3</sub> F <sub>8</sub>	DSPC: DSPG: DSPE-PEG2000 (molar ratio 21:21:1)	NA	stable 1 h at 37 °C	7.6 min for MB 10,8 min for SPIO-DOX-MB (Sprague Dawley rats 200–250 g)	0.3 MPa ( <i>f<sub>c</sub></i> = 1 MHz; BBB opening without damages)	0.5 MPa (BBB opening with damages)	[109]
gas	C <sub>4</sub> F <sub>10</sub>	DSPC: DSPE-PEG2000 (molar ratio 9:1) or DSPC: DSPE-PEG2000-Amine (molar ratio 9:1) or DSPC: DSPE-PEG2000-Amine: DSTAP (molar ratio 7:1:2)	half-life of 2 h	NA	NA	NA	NA	[39]

Table 3. Cont.

Phase	Core	Shell	Storage Stability	In Vitro Acoustic Stability (Echography)	In Vivo Half-Life	Stable Cavitation Threshold	Inertial Cavitation Threshold	Ref.
gas	C <sub>5</sub> F <sub>12</sub>	PEGGM-PDSGM	NA	stable after 14 days at 37 °C half-life at 37 °C	10 min (mice 25–35g) C <sub>3</sub> F <sub>8</sub> : 130 ± 50 s	NA	NA	[88]
gas	C <sub>3</sub> F <sub>8</sub> or C <sub>4</sub> F <sub>10</sub> or SF <sub>6</sub>	DSPC: DSPG: DSPE-PEG2000 (molar ratio 30:60:10)	NA	C <sub>3</sub> F <sub>8</sub> : 80 ± 5 s C <sub>4</sub> F <sub>10</sub> : 145 ± 35 s SF <sub>6</sub> : 20 ± 5 s	C <sub>4</sub> F <sub>10</sub> : 190 ± 40 s SF <sub>6</sub> : 20 ± 20 s	NA	NA	[68]
gas	C <sub>4</sub> F <sub>10</sub>	DSPC: DSPE-PEG2000 (molar ratio 9:1)	Stable 21 days	NA	NA	NA	NA	[102]
gas	C <sub>3</sub> F <sub>8</sub>	DSPC: DSPG: DSPE-PEG2000 (molar ratio 10:4:1)	relatively stable 60 min at 25 °C	NA	NA	0.3 MPa ( $f_c = 1$ MHz; BBB opening without damages)	0.5 MPa (BBB opening with damages)	[125]

$f_c$  = central frequency; NA = Non-assessed; VT: Vaporization threshold; SPIO-DOX-MB: superparamagnetic iron oxide–doxorubicin–microbubble complex; Core compositions: C<sub>3</sub>F<sub>8</sub>: octafluoropropane; C<sub>4</sub>F<sub>10</sub>: decafluorobutane; C<sub>5</sub>F<sub>12</sub>: dodecafluoropentane; C<sub>6</sub>F<sub>12</sub>: perfluoromethylcyclopentane; SF<sub>6</sub>: sulphur hexafluoride; Shell compositions: DBPC: 1,2-dibehenoyl-sn-glycero-3-phosphocholine; DPPA: 1,2 dipalmitoyl-sn-glycero-3-phosphate; DPPC: 1,2-dipalmitoyl-sn-glycero-3-phosphocholine; DPPE: 1,2-dipalmitoyl-sn-glycero-3-phosphoethanolamine; DPTAP: 1,2-dipalmitoyl-3-trimethylammonium-propane; DSPC: 1,2-distearoyl-sn-glycero-3-phosphocholine; DSPE-PEG2000: 1,2-distearoyl-sn-glycero-3-phosphoethanolamine-N-[methoxy(polyethyleneglycol)-2000]; DSPE-PEG2000-Amine: 1,2-distearoyl-sn-glycero-3-phosphoethanolamine-N-[amino(polyethyleneglycol)2000]; DSPG: 1,2-distearoyl-snglycero-3-phospho-rac-glycerol; DSTAP: 1,2-distearoyl-3-trimethylammonium-propane; PEGGM-PDSGM: poly(ethylene glycol-g-glutamate)-co-poly(distearin-g-glutamate); PEG-PLGA: poly(ethylene glycol)-poly(lactide-co-glycolic acid).

Several parameters may influence the bubbles/droplets circulation time as well as the cavitation threshold. For this reason, aspects such as size, chemical composition, shell properties (such as surface tension, elasticity, thickness, surface chemistry), and core properties (molecular weight, density, and boiling point for droplets) have to be taken into account when designing a new agent for FUS-induced BBB opening purpose [127–129]. Concretely, air, nitrogen, and mostly PFC and SF<sub>6</sub> are used as the core gases, while surfactants, lipids, proteins, polymers, or a combination of these materials are used for the shell. For that matter, Figure 4 schematically represents the different possibilities of BBB disruption agent composition.



**Figure 4.** Schematic illustration of most commonly used materials for shell and core composition of agents used for FUS-induced BBB. (C<sub>3</sub>F<sub>8</sub>: octafluoropropane; C<sub>4</sub>F<sub>10</sub>: decafluorobutane; C<sub>5</sub>F<sub>12</sub>: dodecafluoropentane; C<sub>6</sub>F<sub>12</sub>: perfluoromethylcyclopentane; SF<sub>6</sub>: sulphur hexafluoride; N<sub>2</sub>: nitrogen).

### 2.3.1. Bubble or Droplet?

The most commonly used agents for BBB opening with FUS are lipid-shelled microbubbles. PCCA is an attractive alternative to conventional microbubbles. Apart from the core phase, PCCA composition is very similar to that of bubbles [31]. Moreover, stable droplets can be generated through the condensation of commercial PFC bubbles [130]. Like their gas-core counterparts, PCCA is nontoxic at low doses [131]. The shell's surface tension creates a pressure difference between the internal and external environment, known as the Laplace pressure. This pressure allows the compounds to remain stable in the bloodstream [128] until reaching vaporization conditions (i.e., increased temperature and rarefactional acoustic pressure) [131,132].

PCCA presents a significantly longer circulation time *in vivo* than microbubbles since the liquid core prevents gas dissolution [128]: depending on the choice of PFC, droplets may persist stably for hours *in vivo* [133]. Due to their smaller size, PCCA can also potentially extravasate in the leaky vasculature within tumors, unlike microbubbles [31,80,133].

The ultrasound frequency can be tuned to reduce the pressure amplitude required for droplet vaporization (ADV) [134]. Concretely, the vaporization threshold decreases with increasing signal frequency, meaning that a large number of droplets will be activated using high excitation frequency. Conversely, the use of high frequency will increase the shell rupture threshold of bubbles (resulting

in inertial cavitation) [135], decreasing the risk of potential damages. Therefore, increasing the frequency looks promising for the safe application of UCA-mediated therapeutic ultrasound. However, FUS-induced BBB opening is usually performed at low frequency (from 0.2 to 3 MHz) to reduce the ultrasound beam's attenuation through the skull. Another option to reduce the PCCA vaporization threshold would consist of the formulation of low-boiling point droplets at the stability's expense, as described in the following section [131].

In our literature search, the BBB disruption with PCCA has been achieved only three times [33,80,133]. Chen et al. firstly demonstrated BBB disruption with lipid-shelled and  $C_4F_{10}$  core PCCA and successfully delivered 3 kDa dextran to C57BL/6 mice brain without damages. Interestingly, they showed that PCCA had a higher BBB opening pressure threshold (0.450 MPa vs. 0.225 MPa) than the same material microbubbles [133]. In the first study using polymeric PCCA (PEGylated-PLGA shell and  $C_5F_{12}$  core) for BBB opening, Zhang et al. demonstrated that their PCCA has better-focusing abilities than lipid shelled microbubbles (distribution pattern of Evans Blue extravasation on Figure 5) [80], thus reducing side effects outside the focal zone [32,80]. More recently, Wu et al. successfully delivered 40 kDa dextran to the C57BL/6 mice brain without damage with lipid shelled PCCA [33].

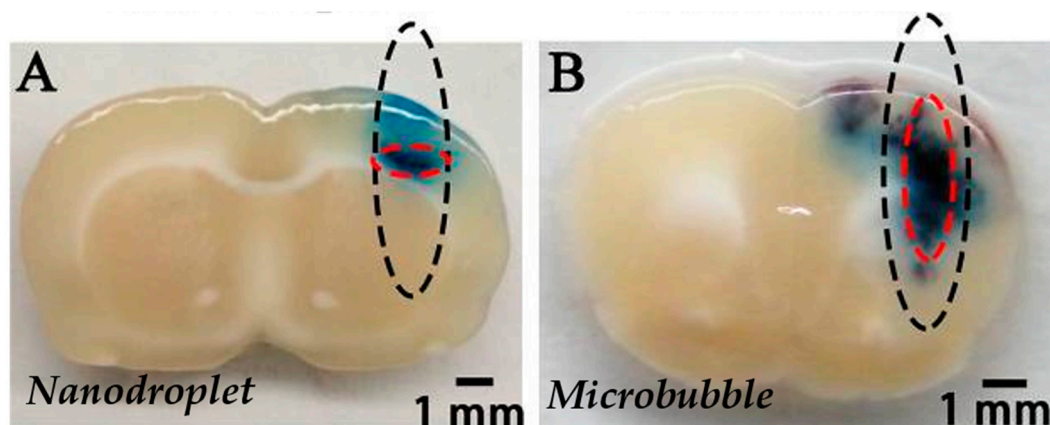


**Figure 5.** Distribution pattern of Evans blue extravasation when PEG-PLGA- $C_5F_{12}$  nanodroplets (A) or lipid microbubbles (B) were used for BBB opening with FUS on male Sprague-Dawley rats. The black dotted circles show the half-maximum of the pressure amplitude of the focal zone. The red dotted circles show the deep blue region of EB extravasation, which indicates the location of the BBB opening. Extracted from Zhang et al. [80], Impact Journals, 2017.

Recently, “acoustic clusters,” produced by electrostatic complexation between negatively charged bubbles and positively charged droplets, have been evaluated for BBB disruption [79]. Indeed, Åslund et al. demonstrated that acoustic clusters made from Sonazoid<sup>®</sup> microbubbles and perfluoromethylcyclopentane microdroplets stabilized with a phospholipid membrane were able to safely and temporarily permeabilize the BBB, using low acoustic pressure and deliver a larger amount of Omniscan<sup>™</sup> (about 30% increase of the gadodiamide signal ratio between the treated part and the non-treated contralateral part of the brain) and 45 kDa molecules into the rat brain in comparison with Sonazoid<sup>®</sup> microbubbles. Briefly, after intravenous injection of the clusters, ultrasound is applied, and the microbubbles transfer the acoustic energy to the attached droplets, which undergo ADV. The acoustic energy transfer enables the microdroplet's liquid-to-vapor phase transition at low acoustic pressure (0.28 MPa in the Åslund et al. study). The resulting acoustic-cluster-bubbles undergo a rapid expansion to approximately 25  $\mu\text{m}$  and transiently deposit in the local microvasculature, stopping the blood flow for up to 10 min. This activated bubble is in direct contact with the endothelial wall ensuring optimal coupling between the vessel wall and the oscillating bubble. The application of ultrasound (0.09 MPa; 1 MHz in the Åslund et al. study) increased the vasculature's local permeability

(Omniscan™ signal in the treated part was 50% higher compared to the non-treated part of the brain in the Åslund et al. study). The acoustic-cluster-bubble stays for typically 10 min, prolonging the treatment time window compared to regular contrast microbubbles [79]. While this approach is innovative, it might be deleterious to stop the blood flow for up to 10 min in the sonicated area.

### 2.3.2. Core Composition

The gas chosen for the core must be non-toxic, hydrophobic, and must have a low solubility to prevent gas leakage through the agent's shell. Heavy gases are preferentially used because bubbles made out of them possess a longer half-life [129,136]. Sulfur hexafluoride (molecular weight, MW = 146.06 g/mol), air (MW = 28.98 g/mol), octafluoropropane (MW = 188.02 g/mol), dodecafluoropentane (MW = 288.03 g/mol), or decafluorobutane (MW = 238.03 g/mol) are often used since their biocompatibility is reported [137]. The PFC must be selected considering the ultrasound pressure needed to induce safe BBB disruption, and in the case of PCCA, the ADV threshold [138]. Acoustic pressure consideration for vaporization or cavitation threshold is crucial for large animal and human applications, as the transmission of high acoustic pressure through the skull remains challenging and requires the use of very sophisticated and expensive ultrasound devices [127].

The Laplace pressure, defined as the differential pressure between the outside and the inside of the droplet, prevents the spontaneous vaporization of the PFC droplets in vivo.

$$\Delta P = P_{inside} - P_{outside} = \frac{2\gamma}{r}$$

where  $\gamma$  is the surface tension, and  $r$  is the bubble/droplet radius. The hydrophobicity of liquid PFC leads to relatively high surface tension, thereby increasing the boiling point. After ADV, the droplet becomes a larger bubble, which remains stable due to the low solubility of the PFC [128]. Thus, depending on the boiling point of the selected materials, droplets can vaporize at different acoustic pressures; the use of PFC with lower boiling points results in easier vaporization at lower acoustic pressures [32].

Omata et al. developed several gas-loaded microbubbles with identical shell compositions and assessed their stability and the effects of the encapsulated gas on BBB opening and drug delivery to the brain. They have also compared those self-made microbubbles to commercial ones (Sonazoid and SonoVue) on the same specifications [68]. The main results of this study are presented in Table 4. The in vitro half-life results suggest that the rank order of gas-bubble stability in vitro, from the longest to the shortest, is C<sub>4</sub>F<sub>10</sub>, C<sub>3</sub>F<sub>8</sub>, and SF<sub>6</sub>. The in vivo experiments were performed on mice kidneys and suggested the same tendency, except for the Sonazoid bubbles that appear to be less stable in the circulation despite their high stability in vitro. Omata et al. suggest that this is due to Sonazoid shell composition, which contains hydrogenated egg phosphatidylserine, a lipid known to be rapidly uptake by some liver cells. On the BBB opening and drug delivery assessments, C<sub>3</sub>F<sub>8</sub> and C<sub>4</sub>F<sub>10</sub> cores continue to show the best performances. Moreover, all the BBB disruption was reached without damages. Sonazoid resulted in high Evans blue delivery despite its short in vivo half-life. For this reason, Omata et al. repeated the BBB opening assessment for Sonazoid and C<sub>3</sub>F<sub>8</sub> and C<sub>4</sub>F<sub>10</sub> self-made bubbles but applying ultrasound 3 min after injection. Under these conditions, Evans blue leakage was still observed on the brain's sonicated part, but the difference with the untreated part of the brain was not significant for the Sonazoid bubbles. The study concluded that self-made C<sub>3</sub>F<sub>8</sub> and C<sub>4</sub>F<sub>10</sub> were more stable and efficient for BBB opening and drug delivery.

**Table 4.** Comparison of different bubbles on their stability and their abilities to open the BBB and deliver 70 kDa fluorescent dextran to the brain performed by Omata et al. [68].

Commercial Name	Bubble Characteristics			Stability Assessments *			BBB Opening Performances		
	Shell	Core	Average Size (µm)	In Vitro Half-Life at 37 °C (s)	In Vivo Half-Life (s)	Injection (µL/kg)	Evans Blue Leakage (µg/g Brain) *		70 kDa Dextran Delivery
							<i>t</i> <sub>US</sub> = 0 s	<i>t</i> <sub>US</sub> = 3 min	
Sonazoid (GE Healthcare)	lipid	C <sub>4</sub> F <sub>10</sub>	2.11 ± 0.02	1300 ± 250	40 ± 20	3333	18 ± 7	3.2 ± 0.5	NA
SonoVue (Bracco)	lipid	SF <sub>6</sub>	2.23 ± 0.02	60 ± 10	20 ± 10	30,000	5 ± 1	NA	NA
NC	DSPC: DSPG:	C <sub>3</sub> F <sub>8</sub>	1.48 ± 0.02	80 ± 5	130 ± 50	1875	13 ± 3	3.5 ± 1.5	high fluorescence
NC	DSPE-PEG2000 (molar ratio 30:60:10)	C <sub>4</sub> F <sub>10</sub>	1.36 ± 0.02	145 ± 35	190 ± 40	1875	10 ± 1	4.2 ± 0.2	high fluorescence
NC		SF <sub>6</sub>	1.63 ± 0.01	20 ± 5	20 ± 20	5000	4 ± 1	NA	weak fluorescence

NC: Non-commercial; *t*<sub>US</sub>: delay time of ultrasound exposure after bubble injection; C<sub>3</sub>F<sub>8</sub>: octafluoropropane; C<sub>4</sub>F<sub>10</sub>: decafluorobutane; SF<sub>6</sub>: sulphur hexafluoride DSPC: 1,2-distearoyl-sn-glycero-3-phosphocholine; DSPG: 1,2-distearoyl-sn-glycero-3-phosphoglycerol; DSPE-PEG2000: N-(carbonyl-methoxypolyethyleneglycol 2000)-1,2-distearoyl-sn-glycero-3-phosphoethanolamine; NA: Non-assessed. Acoustic parameters: Intensity = 0,5 W/cm<sup>2</sup>; *f*<sub>c</sub> = 3 MHz; duration = 180 s; burst = 100 s. \* data obtained by graphical reading.

Concerning the PCCA core, Wu et al. compared two low-boiling point PCCA for their abilities to disrupt the BBB and deliver dextran molecules to the murine brain. Octafluoropropane (boiling point  $-36.7\text{ }^{\circ}\text{C}$ ) PCCA successfully delivered 40-kDa dextran to the brain at 300 kPa and 450 kPa without evidence of cavitation damage. Using decafluorobutane (boiling point  $-1.7\text{ }^{\circ}\text{C}$ ) PCCA, the successful delivery of dextran at 900 kPa was associated with tissue damage due to inertial cavitation. Interestingly, no delivery was detected at a lower pressure of 750 kPa [33]. No study reported PCCA made with a sulfur hexafluoride core (boiling point is  $-68.25\text{ }^{\circ}\text{C}$ ). Those PCCA would probably not be stable enough to be injected in vivo. Those studies' results are very informative and suggest that the comparison of core compositions repercussions on stability, acoustic responsiveness, and BBB opening ability should be further investigated.

### 2.3.3. Shell Composition

A proper shell must balance flexibility and sturdiness: it has to be flexible enough to let the bubble oscillate at relatively low acoustic pressure while having a proper surface tension to prevent gas leakage from the core or keep it in its liquid form at physiological temperature for droplets.

The most elastic shells are made of phospholipids, while the stiffer ones are made of polymers or proteins [30]. Lipid-shelled microbubbles are highly responsive to ultrasound, while the polymer and protein-shelled microbubbles are very stable and require higher acoustic pressure to undergo cavitation [24,139]. PEG-surfactants are systematically used with phospholipid shells due to their ability to appreciably lower surface tension [102]. Other surfactant shells have also been explored in echogenic contrast agent fabrication [128].

Wu et al. examined the effects of lipid acyl chain lengths (C16, C18, C24) for molecular delivery to the murine brain after BBB disruption. Increasing lipid tail length and its shell rigidity resulted in a significant increase in the delivery of 40-kDa dextran. The difference in molecular delivery between the different shells was weaker with higher pressure [92].

Pouliopoulos et al. compared different lipid shell microbubbles shelled on their acoustic stability in vitro [102]. The shells were composed of 1,2-distearoyl-sn-glycero-3-phosphocholine (DSPC) and 1,2-distearoyl-sn-glycero-3-phosphoethanolamine-*N*-[methoxy(polyethylene glycol)2000] (DSPE-PEG2000) with different molar ratio (6:1; 9:1; and 12:1). The bubbles were excited with a 0.5 MHz FUS transducer, and passive cavitation detection was performed with a 7.5 MHz single element FUS transducer. The energy transmitted by the excited bubble was processed to appraise the different shell acoustic stabilities. Eventually, a 9:1 ratio was found to provide higher acoustic stability [102]. DSPC:DSPE-PEG2000 at a molar ratio of 9:1 is the most commonly formulated lipid shell for microbubble self-made for BBB disruption.

The electrical charge of the shell can also influence its properties. Cationic bubbles have been explored for BBB opening [104–106] due to their ability to form electrostatic complexes with negatively charged molecules such as nucleic acids (DNA, RNA, oligonucleotides) [30]. Besides, cationic bubbles have shown some advantages compared to neutral bubbles. Even though it might be cleared by the organism faster than neutral bubbles [30], it can conversely present better stability below  $37\text{ }^{\circ}\text{C}$  when the cationic lipid used for the shell has a higher transition temperature than the neutral one [107]. Tan et al. compared three lipid bubbles with different surface charges (neutral: Neu, slightly cationic: Scat, and cationic: Cat) with neutrally charged Definity microbubbles in vitro by performing shell elastic modulus and turbidity measurements and by evaluating their ability to increase the permeability of epithelial brain cells [39]. The different surface charges were obtained by varying the lipid compositions and the chemical termini of the lipid shell. Neu bubbles were formulated at a 9:1 molar ratio of DSPC:DSPE-PEG2000, Scat bubbles were formulated at a 9:1 molar ratio of DSPC and 1,2-distearoyl-sn-glycero-3-phosphoethanolamine-*N*-[amino(polyethylene glycol)2000] (DSPE-PEG2000-Amine), and Cat bubbles were formulated at a 9:2:1 molar ratio of DSPC, DSPE-PEG2000-Amine, and 1,2-distearoyl-3-trimethylammonium-propane (DSTAP). All the bubbles were about the same size (around  $1\text{ }\mu\text{m}$ ), and the average Zeta potential measured was  $-10.6 \pm 0.8\text{ mV}$ ,

17.0 ± 0.3 mV, 29.8 ± 0.3 mV, −1.1 ± 0.2 mV for the Neu, Scat, Cat, and Definity bubbles, respectively. The shell elastic modulus was higher for Definity bubbles and similar for the three homemade bubbles suggesting that (i) Definity bubbles have a higher cavitation threshold than the homemade agents and (ii) the bubble surface charge does not influence its elasticity. Turbidity measurements showed that after 5 min sonication ( $f_c = 3$  MHz; MI = 0.8), the number of bubbles remaining in the water bath was lower for SCat bubbles (20%) than for the others (Neu: 40%; Cat: 80%; Definity: ~100%) suggesting that the SCat bubbles have the lowest inertial cavitation threshold as they were more deteriorated than the other type of bubbles. Finally, cell permeability to 70-kDa dextran assessment showed best results for the Scat bubbles which might be explained by their lower cavitation threshold and electrostatic interactions between their cationic shell and the negatively charged cell membranes. Based on these results, SCat bubbles were evaluated for BBB disruption in vivo.

Once again, we believe that shell composition repercussions on stability, acoustic responsiveness, and BBB opening performances must be further studied.

### 2.3.4. Fabrication Methods

The agent used for BBB disruption can be made with several methods. The three most common bubbles fabrication methods are sonication, shaking, and microfluidics [140]. Sonication is performed with a high-frequency vibration (typically 20 kHz) horn tip at the gas/water interface. Shaking is another mechanical agitation process consisting of a device vibrating along the long axis of a vial at 4000 Hz. This method is used to generate Definity<sup>®</sup> microbubbles, for example. Sonication and shaking produce polydisperse microbubbles very rapidly and economically. If a monodisperse distribution of the bubble solution is desired, the solution can be centrifugally sorted at the yield's expense. Moreover, sonication can produce larger amounts of bubbles than shaking. Microfluidic methods, which have been more recently proposed, are interesting because they produce monodisperse microbubbles and offer directed assembly for more sophisticated structures. However, those methods have relatively slow rates, and they are difficult and expensive to employ.

Sheeran et al. reported the following techniques for the fabrication of phase-change PFC droplets: shaking, sonication, extrusion, condensation, and microfluidic techniques [141]. As for bubble fabrication, shaking methods can achieve micro-scale emulsions simply and rapidly but produce a broad size distribution and have low reproducibility between batches. In contrast, sonication techniques can produce nano-scale droplets with a narrower size distribution but may require size exclusion processes such as filtration. Microfluidic techniques offer a much narrower size distribution, but the ease and speed of manufacture may be limited [128]. Among the PCCA used for BBB disruption, microbubble condensation [33,133], and double sonication method [80] have been used. The condensation method requires to decrease the ambient temperature and raise the ambient pressure of the microbubble suspension. This technique enables the simple production of high-concentration PCCA and offers the possibility of modifying and manipulating microbubbles at the microscale prior to condensation. However, this method produces polydisperse droplets if the preceding microbubble suspension is highly polydisperse (however, differential centrifugation can be performed to overcome this) [141]. The fabrication method is essential as it impacts the agent size distribution and concentration of the suspension.

### 2.3.5. Size Distribution and Concentration

Concentration and bubble size influence their dissolution and clearance rate [127]. Indeed, as Borden et al. described, the lipid monolayer bubble's dissolution rate increases with decreasing bubble size. Thus, smaller microbubbles dissolve faster than larger ones [140]. Sirsi et al. demonstrated that increasing bubble diameter and/or concentration increases in vivo circulation persistence by comparing bubbles of different sizes (1–2 µm; 4–5 µm and 6–8 µm) and at different concentrations (between 10<sup>7</sup> and 10<sup>9</sup> bubbles/mL) [142]. However, for intravenous administration, the microbubble diameter must be smaller than 6 µm [30]. Cheng et al. also studied submicronic bubbles (288 ± 17.6 nm)

stability regarding the concentration and observed that the in vitro persistence was higher with a higher concentration (concentration ranging between  $10^7$  and  $10^{11}$  bubbles/mL) [108].

While the droplet vaporization threshold is inversely proportional to droplet diameter [128], it has also been demonstrated that bubble cavitation behavior depends on its size. Indeed, smaller bubbles were more susceptible to destruction by fragmentation under acoustic stimulation [143]. Moreover, Choi et al. showed that increasing the bubble diameter decreased the cavitation thresholds (0.30 and 0.46 MPa for 1–2  $\mu\text{m}$  bubbles and 0.15 and 0.30 MPa for 4–5  $\mu\text{m}$  bubbles) and that BBB opening is higher with larger diameter bubbles for every pressure tested [144]. However, Bing et al. have observed in vivo ultra-harmonic emission at lower acoustic pressure for submicronic bubbles ( $288 \pm 17.6$  nm; 0.23 MPa) in comparison to Definity and Optison microbubbles ( $\sim 2$   $\mu\text{m}$ ; 0.34 MPa and 0.42 MPa respectively), suggesting that BBB opening might be achieved with the high activity of submicronic bubbles under relative lower focal pressures. The authors noted that this observation might differ from Choi et al. study due to the relatively high concentration of the submicronic bubbles (737  $\mu\text{L}/\text{kg}$ ). As a result, part of the bubbles may combine and form a cluster with a larger diameter compared to both Optison and Definity [38].

#### 2.4. Bimodal Ultrasound-MRI Contrast Agents for BBB Disruption

MRI is currently used to guide and evaluate the efficiency of therapeutic ultrasound procedures. It allows precise targeting, identification of the lesion, and dynamic feedback on the extent of BBB disruption via MR contrast leakage [1,18]. Two types of agents are used to enhance the contrast on MR images: (i) paramagnetic agents, which consist of a chelate with a paramagnetic core (usually gadolinium) or (ii) superparamagnetic agents composed of iron oxide nanoparticles coated with a hydrophilic organic protective layer such as dextran [145].

Most of the studies reported the use of paramagnetic agents made of gadolinium chelates commercially available such as Gadovist<sup>®</sup> (Gd-DO3A-butrol), Dotarem<sup>®</sup> (Gd-DOTA), Magnevist<sup>®</sup> (Gd-DTPA), Omniscan<sup>®</sup> (Gd-DTPA-BMA), and Multihance<sup>®</sup> (Gd-BOPTA) that are co-administered with the UCAs. Aryal et al. incorporated a gadolinium-labeled lipid in the lipid bilayer of liposomes injected as an MRI contrast agent. After BBB opening on mice with Optison<sup>®</sup> microbubbles, the signal intensity was slightly higher on longitudinal relaxation time (T1)-weighted images for the sonicated hemisphere than the control volume, indicating that the gadolinium-labeled liposomes were effectively delivered to the brain and visible on MR images. Two different sizes of liposomes were compared (77.5 nm and 140 nm), and the relative increase in MRI signal intensity was greater for smaller liposomes than larger ones [70].

Conventional UCAs have also been used for MRI [146] due to the gas-liquid interface producing large local magnetic susceptibility differences visible in transversal relaxation time (T2)-weighted MR images. For that matter, Cheung et al. used two types of bubbles (custom-made air-filled and albumin-coated microbubbles and SonoVue<sup>®</sup> microbubbles) for in vivo dynamic brain MRI in Sprague-Dawley rats. Transverse relaxation rate enhancements were observed in the brain after bubbles intravenous injection [147].

The microbubble response can be further enhanced by incorporating paramagnetic or superparamagnetic particles into their shells, giving rise to multimodal contrast agents used for BBB disruption and dynamic contrast-enhanced MRI. Liao et al. reported the use of perfluorocarbon-filled albumin-(Gd-DTPA) microbubbles for monitoring FUS-induced BBB opening [148]. T1-weighted MRI confirmed the BBB disruption, and T2-weighted MRI allowed to detect intracerebral hemorrhage. Besides, Fan et al. formulated a multimodal, therapeutic, and active-targeting microbubble encapsulating a superparamagnetic iron oxide-doxorubicin (SPIO-DOX) complex. The lipid microbubble filled with perfluoropropane successfully opened the BBB upon sonication, and the magnetic activation of SPIO nanoparticles triggered the release of chemotherapeutic agent DOX into rat glioma. Figure 6 schematically represents the SPIO-DOX-microbubble complex, the SPIO deposition as a function of  $1/T_2$  values in MR images, and the DOX deposition into the rat brain as a function of

the treatment used. The SPIO deposition into the rat brain tumor was correlated with differences in  $1/T_2$  values in MR images ( $r^2 = 0.83$ ) and with DOX deposition ( $r^2 = 0.79$ ), supporting the theranostic capabilities of the SPIO-DOX-microbubble complex [109].

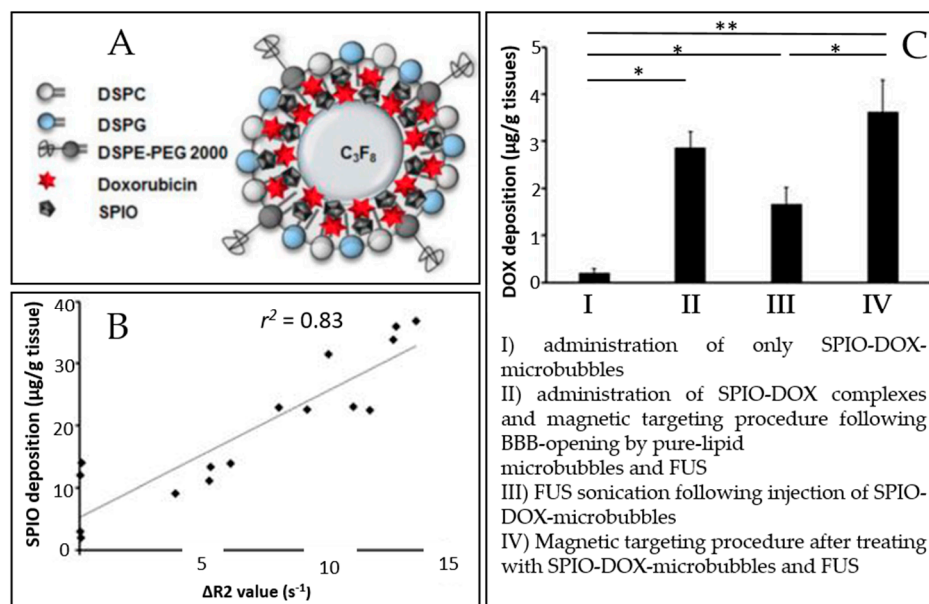


**Figure 6.** An example of a multimodal agent for BBB disruption, MRI, and drug delivery purposes (extracted from Fan et al. [109], Ivyspring International Publisher, 2016). (A) Illustration of SPIO-DOX-microbubble structure. (B) Correlation between SPIO deposition and  $\Delta R_2$  value. (C) DOX accumulation measured by high-performance liquid chromatography. \*:  $p < 0.05$ ; \*\*:  $p < 0.01$ .

PFC droplets can theoretically be observed on  $^{19}\text{F}$  MRI since it has been reported in vitro [149]. Nevertheless, in vivo  $^{19}\text{F}$  MRI imaging remains challenging due to the low PFC quantities available in the brain after BBB disruption.

## 2.5. Drug Delivery and Targeting

This section is focused on microbubble-assisted drug delivery and targeting strategies to the brain recently exploited. Exhaustive reviews already detail the different possibilities for drug delivery to the brain in conjunction with FUS [34,150]. Some of them are specifically dedicated to cancer treatment [151,152] or gene delivery and targeting [30].

### 2.5.1. Targeting

Localized BBB opening can be achieved using physical stimuli (such as FUS or magnetic field), while functionalized agents with a ligand can target overexpressed receptors associated with the treated pathology.

Fan et al. used magnetic targeting as a physical targeting option: particles can be magnetized and become physically sensitive to external magnetic fields. This approach was validated in vivo using the SPIO-DOX-microbubble complex described earlier (schematically represented in Figure 6A). It increased SPIO deposition in the rat brain by 2.8 fold [109]. As well, Wu et al. made lipid-shelled bubbles conjugated with cationic polyethylenimine-coated super paramagnetic iron oxide particles (PSPIO) to open the BBB on mice. The SPIO, here again, was used for magnetic targeting and enhanced the BBB opening by 2.8-fold compared with unconjugated bubbles [125].

Molecular targeting of the circulating microbubbles would allow a BBB opening in the desired area without affecting healthy tissues. Typical ligands used for molecular targeting are antibodies

or peptides. Table 5 summarizes the different molecular targeting and drug/gene-complexed bubble options for BBB opening and therapeutic purposes found in the recent literature.

**Table 5.** Molecular targeting and drug/gene-complexed bubble for BBB opening and therapeutic purpose.

Ref	Core	Shell	Molecular Targeting	Drug/Gene Embedded in the Agent
[86]	air	polymer	NA	quercetin-modified sulfur nanoparticles-loaded bubble
[88]	C <sub>5</sub> F <sub>12</sub>	polymer	des-octanoyl ghrelin-conjugated bubble	TGFβ1 inhibitor (LY364947)-loaded bubble
[89]	SF <sub>6</sub>	lipid	NA	<i>GDNFp</i> / <i>BDNFp</i> -loaded liposome bound to bubble
[90]	SF <sub>6</sub>	lipid	NA	ultrasound-sensitizing dye-incorporating nanoparticles bound to bubble
[110]	C <sub>3</sub> F <sub>8</sub>	lipid	NGR-conjugated (targeting)/ <i>shBirc5</i> -loaded (gene) liposome bound to bubble	
[104]	C <sub>3</sub> F <sub>8</sub>	lipid	anti-VEGFR2 antibody-conjugated bubble	<i>pLUC</i> / <i>pHSV-TK/GCV</i> -loaded bubble
[109]	C <sub>3</sub> F <sub>8</sub>	lipid	NA	SPIO-DOX-conjugated bubble
[111]	C <sub>3</sub> F <sub>8</sub>	lipid	NA	<i>GDNFp</i> -loaded cationic bubble
[112]	C <sub>3</sub> F <sub>8</sub>	lipid	NA	<i>pDC315/Nrf2</i> -loaded bubble
[107]	C <sub>3</sub> F <sub>8</sub>	lipid	folate-conjugated bubble	<i>pLUC</i> -loaded bubble
[105]	C <sub>3</sub> F <sub>8</sub>	lipid	NA	<i>pPrestin</i> -loaded bubble
[106]	C <sub>3</sub> F <sub>8</sub>	lipid	NA	boron-containing polyanion nanoparticles coupled with cationic bubble
[125]	C <sub>3</sub> F <sub>8</sub>	lipid	NA	PSPIO- <i>GDNFp</i> -loaded bubble
[113]	C <sub>3</sub> F <sub>8</sub>	lipid	phosphatidylserine nanoparticles-microbubble complex	

TGFβ1: transforming growth factor; *GDNFp*: a glial cell line-derived neurotrophic factor plasmid DNA; *BDNFp*: brain-derived neurotrophic factor plasmid DNA; NGR: Asn-Gly-Arg peptide; *shBirc5*: short hairpin RNA-*Birc5* gene; VEGFR2: vascular endothelial growth factor receptor 2; *pLUC*: plasmid DNA encoding luciferase gene; *pHSV-TK/GCV*: plasmid DNA encoding herpes simplex virus type 1 thymidine kinase/ganciclovir gene; SPIO-DOX: superparamagnetic iron oxide-doxorubicin complex; *pDC315/Nrf2*: plasmid DNA encoding DC315-nuclear factor E2-related factor 2; *pPrestin*: plasmid DNA encoding Prestin protein; *PSPIO-GDNFp*: superparamagnetic iron oxide coated with cationic polyethylenimine conjugated with plasmid DNA encoding glial cell line-derived neurotrophic factor; NA: Not applicable).

Chen et al. developed des-octanoyl ghrelin-conjugated microbubbles loaded with TGFβ1 inhibitor to disrupt BBB on glioma-bearing mice. Des-octanoyl ghrelin is a ligand that can bind with BBB. Authors have observed higher BBB disruption with the des-octanoyl ghrelin-conjugated microbubbles than the unconjugated ones (negative contrast intensity of superparamagnetic iron oxide nanoparticles on the T2-weighted MRI images was 0.81-fold higher for the conjugated microbubbles) [88].

Specific biomarkers of the blood-tumor barrier (BTB) could be used to target microbubbles toward these tumors. Indeed, gliomas and brain metastases are tumors known to compromise the integrity of the BBB, resulting in a vasculature known as the BTB, which is highly heterogeneous and characterized by numerous distinct features, including non-uniform permeability and active efflux of molecules [153]. Vascular endothelial growth factor receptor 2 (VEGFR2) is one of the selected targets as it is a specific endothelial molecular marker of angiogenesis, which is exceptionally high in tumor growth and, thus, overexpressed in BTB [154]. Moreover, the inhibition of VEGFR2 with antibodies results in prolonged survival in cancer patients [154]. Functionalized bubbles/droplets with VEGFR2-targeted ligand were formulated for BTB targeting. Chang et al. have used anti-VEGFR2 antibody-conjugated cationic microbubbles to target VEGFR2 in the rat BTB. The microbubble targeting efficiency was evaluated in vitro on C6 glioma cells and was  $99.4 \pm 0.3\%$ , while it was  $6.4 \pm 1.2\%$  for unconjugated microbubbles [104]. Most of the targets studied, such as VEGFR2, are directed to endothelial cells. However, it is also possible to target receptors directly expressed on the malignant cells, i.e., folate receptors. Hence, Fan et al. used this receptor as a target for BBB opening and gene delivery in the C6 glioma rat model. They have demonstrated the targeting ability on C6 glioma cells of folate-conjugated DNA-loaded cationic microbubbles in vitro: the folate increased the targeting ability of the complex by 7.6 fold [107]. Besides, Zhao et al. used Asn-Gly-Arg (NGR), a peptide motif that can be used to target CD13 receptors. CD13 is overexpressed in glioma cells and neovascular endothelial cells. In vitro, NGR-linked-*shBirc5*-loaded liposome complex linked to lipid-shelled microbubble

demonstrated a better *shBirc5* gene transfection on C6 glioma cells for the targeted microbubble compared to the untargeted ones (36.25% of transfection efficiency vs. 21.26%), thereby demonstrating the targeting profits [110].

Molecular targeting was always associated with drug/gene loaded into the bubble in the browsed literature. Indeed, molecular targeting may improve drug delivery: Fan et al. have observed better gene transfection efficiency in vivo for their folate-conjugated microbubbles than those without conjugation (luciferase gene expression 4.7 fold higher after 24 h) [107].

### 2.5.2. Drug and Gene Delivery

Drug delivery through the BBB with FUS can be reached by (i) co-injection of microbubbles and free drugs or drug carriers or (ii) encapsulating or covalently linking the therapeutics to the agent shell [32,129]. Loading drugs into the shells of microbubbles enables better spatial control to deliver the drug to the treated site. The encapsulation of the drug would also decrease the side effects induced by the circulation of a high drug dose in the vasculature [30,32].

Non-viral gene delivery by plasmid DNA complexation with bubbles was studied in numerous studies [89,104,105,107,110–112]. Thereby, glial cell line-derived neurotrophic factor (GDNF) [89,111,125], brain-derived neurotrophic factor (BDNF) [89] and nuclear factor E2-related factor 2 (Nrf2) [112] have been studied for Parkinson's disease treatment. Gene therapy with neurotrophic factors is a promising approach to improving current Parkinson's disease therapy. It has been found to reduce progressive neuronal loss and play a crucial role in the development, survival, and maintenance of the central and peripheral nervous system [89]. Nrf2 is a nuclear factor that activates the antioxidant response element pathway and protects the brain by regulating redox status. Nrf2 might be useful in Parkinson's disease therapy as reactive oxygen species play an important role in disease development [112]. Thus, these factors have been encoded in plasmid DNA and complexed with microbubble for BBB disruption and drug delivery on Parkinson's disease rodent model [89,111,112,125]. Neurotrophic factor delivery provided a neuroprotective effect by showing evidence of improvement of behavioral deficits [89,111,125], while Nrf2 gene transfection enabled the reduction of reactive oxygen species levels [112].

Interestingly, Wu et al. have used *pPrestin*-microbubble to disrupt the BBB, modify, and activate neurons within mice brain for spatiotemporal neuromodulation [105]. Prestin is a transmembrane protein that exists in the mammalian auditory system and functions as an electromechanical transducer. The cellular transfection rate with *pPrestin*-microbubble was 1.5-fold higher than with commercial transfection agents (LT-1) [105].

Chang et al. used anti-tumor suicide gene therapy for glioblastoma therapy on Sprague-Dawley rats using cationic VEGFR2-targeted microbubbles, complexed with luciferase gene and herpes simplex virus type 1 thymidine kinase/ganciclovir (gene suicide system) encoding plasmid DNA (*pLUC* and *pHSV-TK/GCV*). Anti-tumor suicide gene therapy involves tumor-targeted transfection of a suicide gene that encodes an enzyme for converting non-toxic prodrugs into toxic products to kill tumor cells. Both VEGFR2-targeting and *pHSV-TK* contributed to improving the anti-tumor efficiency: 25 days after tumor implantation, the tumor volume was  $9.7 \pm 5.2 \text{ mm}^3$  for the *pHSV-TK/GCV*-loaded VEGFR2-targeted microbubbles-treated group,  $40.1 \pm 4.3 \text{ mm}^3$  for the untargeted *pHSV-TK/GCV*-loaded microbubbles-treated group, and approximately  $68 \pm 8 \text{ mm}^3$  for the untreated group [104].

Another technique of gene delivery therapy is the RNA interference technique, which consists of protein expression inhibition. The RNA interference technique includes small interfering RNA (siRNA) and short hairpin RNA (shRNA). Zhao et al. used this technique on an orthotopic C6 glioma rat model with NGR-conjugated *shBirc5*-loaded liposome attached to microbubbles. *Birc5* is a protein in the family of apoptosis inhibitors. The *Birc5* gene is only expressed in malignant tumors and not in normal tissue. Thus, a plasmid containing shRNA for the *Birc5* gene could enter the cell, decrease *Birc5* gene transcription in a targeted manner, promote tumor cell apoptosis, and reduce angiogenesis without affecting normal cells. The triple function agent (tumor cell targeting, delivering gene, and BBB

opening) in conjunction with FUS exhibited a significant therapeutic effect, higher than the control group: median survival times were 38 and 21 days, respectively [110].

Besides, Chen et al. have proposed another cancer treatment possibility combined with molecular targeting: des-octanoyl ghrelin-conjugated microbubbles were loaded with TGF $\beta$ 1 inhibitor (LY364947). Transforming growth factor TGF $\beta$  plays an essential role in the functional regulation of tumor interstitium; it also controls the permeability of the BBB and reduces the permeability of the brain's endothelial cell. Therefore, inhibition of TGF $\beta$  in cancer cells is expected to improve the therapeutic effects of chemotherapy. Thus, the deposition of doxorubicin in mice brain tissues was higher for the mice treated with TGF $\beta$ 1 inhibitor-loaded conjugated bubbles ( $45 \pm 5 \mu\text{g/g}$  of tissue) than for the group treated with unloaded conjugated bubbles ( $35 \pm 5 \mu\text{g/g}$  of tissue). The median survival time was also increased (44 days for loaded microbubbles, 38 days for unloaded microbubbles) [88].

As mentioned earlier, anti-cancer drug-loaded bubbles have also been explored for cancer treatment (Figure 6) [109]. Interestingly, Fan et al. [106] proposed an alternative to boron neutron capture therapy consisting of radiotherapy based on boron agent delivery to the brain [151]. For a more efficient tumor-targeted delivery of boron, the authors fabricated boron-containing nanoparticles-loaded microbubbles for the treatment of the glioma-bearing mice model. The complex successfully disrupted the BTB and delivered boron into the brain tumor ( $76.6 \pm 3.6\%$  of boron uptake in tumor 4 min after drug delivery) [106].

Several studies came up with other innovative drug delivery. Briefly, Zhao et al. used phosphatidylserine nanoparticles-microbubbles complexes to monitor inflammatory reaction [113]. The complex successfully and safely opened the BBB and activated the microglia/macrophage in the rat brain. In addition, Liu et al. used sulfur nanoparticles-quercetin complex embedded in the microbubble shell for Alzheimer's treatment [86]. Those microbubbles successfully opened the BBB on mice and allowed for a rapid accumulation of nanoparticles-quercetin complex in the brain, leading to improved Alzheimer's disease outcome (significant increase of success on Morris water maze experiment after treatment). Finally, Ha et al. proposed a drug delivery system by binding microbubble with ultrasound-sensitizing dye-incorporating nanoparticles. They successfully delivered those nanoparticles to the U87MG (human glioblastoma cell line) located in the mouse brain (fluorescence intensity 1.5 times higher than the control group) [90].

Among the multifunctional bubbles for drug delivery strategies found in the recent literature, most of them have to be destroyed to release the active principle embedded in their shell. However, bubble destruction results in a significant risk of brain damage (hemorrhage), which is not acceptable. Although safe BBB disruption with no evidence of acute or chronic inflammation was pointed out after bubble destruction by some studies [89,105], DNA delivery has been reported without destroying the DNA-loaded bubble [104]. Indeed, DNA loaded in bubbles might penetrate cells through endocytosis when the bubble undergoes stable cavitation [104].

### 3. Discussion

#### 3.1. Safety

To move forward into clinical trials, newly designed agents for FUS-induced BBB opening have to be safe. Meng et al. provide a synthesis of ultrasound parameters and drug characteristics that influence FUS's safety profile to enhance drug delivery [27]. The safety is reachable in a particular window of parameters, including ultrasound parameters [129], microbubble dose [75,127,155], and the biocompatibility of the materials used to design the agent. The low-intensity ultrasound used for FUS-induced BBB opening is expected to have minimal thermal effects. Negligible temperature elevations ( $<3 \text{ }^\circ\text{C}$ ) were reported in studies with different ultrasound parameters in rats, rabbits, and sheep [27]. Mechanical index (MI) can be used to avoid excessive cavitation of bubbles. MI is defined as the ratio between the peak-negative pressure and the square root of the center frequency ( $f_c$ ) [129]. As for direction, the British Medical Ultrasound Society has set a limit for diagnostic applications

of ultrasound of  $MI = 0.7$  for bubbles. For therapeutic applications, no limitations have been set yet. BBB disruption without hemorrhage has been reported with bubbles (proteins and nanoparticles self-assembled shell with  $C_3F_8$  core) for  $MI = 0.25$  on Sprague Dawley rats, among others [85]. McMahon et al. have demonstrated the bubble dose dependence of inflammatory response after BBB disruption [155]. While a  $10 \mu\text{L}/\text{kg}$  dose of Definity did not show any inflammatory response on the rat brain, a  $100 \mu\text{L}/\text{kg}$  dose resulted in an inflammatory response accompanied by edema, neuronal degeneration, neutrophil infiltration, and micro-hemorrhage.

### 3.2. Ongoing Challenges and Future Directions

To date, twenty-three clinical trials have been (3), are presently (4) or will be (16) conducted to settle a proof of concept of BBB opening with FUS ([clinicaltrials.gov](https://clinicaltrials.gov)) for the treatment of several conditions: glioblastoma or brain metastases (14), Alzheimer disease (6), Parkinson disease (2) and amyotrophic lateral sclerosis (1). To the best of our knowledge, five teams have published the results from those trials in peer-reviewed journals [156–161]. These phases I and IIa clinical trials use clinically approved microbubbles for diagnostic imaging to facilitate the clinical translation of the procedure.

Agents that are not already clinically approved need to fulfill several requirements as sufficient accumulation in the target tissue, biocompatibility, clearance from the body, higher efficacy than clinically-approved microbubbles, cost-effectiveness, large scale production, easy formulation, packaging, and storage [32,128].

Characterization of cavitation thresholds (and vaporization threshold if needed), size distribution, in vivo circulation persistence, and electrical charge measurement of the newly designed agent must be performed whenever used for BBB disruption with FUS. The design of shells that can encapsulate drugs or MR contrast agents or bind with ligands for precise targeting should be further investigated as these approaches present numerous promising leads.

A more recent approach uses gas vesicles present in buoyant microorganisms to engineer theranostic agents. These gas vesicles are protein shell structures with a few hundreds of nanometers that allow coupling focused ultrasound to cells using genetic tools and improve circulation stability due to the carrier cells' intrinsic properties [162–164]. This technology creates a unique opportunity for cell-based therapeutics and diagnostics. Cells can be sonoporated with unprecedented control, for example, to kill cancer cells, release a molecular payload such as drugs, or potentially disrupt the BBB at smaller capillaries in comparison with microbubbles.

## 4. Conclusions

In summary, this review describes the theranostic capability of microbubbles in noninvasive therapeutic ultrasound interventions. The therapeutic applications of microbubbles have been explored in vivo, where the effects of cavitation were linked to drug delivery enhancement in the CNS due to the temporary increase of BBB permeation. We discussed the use of both microbubbles originally designed as imaging contrast agents and microbubbles and droplets engineered specifically for therapy application with increased stability in blood circulation and penetration, as well as the development of multimodal contrast agents used for BBB disruption and dynamic contrast-enhanced MRI. The fabrication methods and agent characterization (microbubbles and droplets) were described in terms of optimal size, concentration, dissolution, clearance rate, and vaporization. We also described the agents' use as carriers for magnetic particles, genes, neurotrophic factors, and anti-cancer drugs, which provide superior spatial control of drug release and higher concentration doses at targeted regions. Finally, the ongoing challenges involved in clinical trials revealed the importance of developing agents and methods based on cavitation monitoring to assess the safety and efficacy during brain treatment. Such developments may potentially include the use of acoustic biomolecules that offer promising results for cell-based therapeutics and diagnostics.

**Author Contributions:** A.D. (Ambre Dauba) performed the literature search and wrote the original draft; A.N. supervised and acquired the funding; A.N., A.D. (Anthony Delalande), N.T., H.A.S.K., A.C., and B.L. reviewed and edited the manuscript. All authors have read and agreed to the published version of the manuscript.

**Funding:** This work was funded by the ANR DROPMUT (grant ANR-19-CE19-0011).

**Conflicts of Interest:** The authors declare no conflict of interest.

## References

1. Burgess, A.; Shah, K.; Hough, O.; Hynynen, K. Focused ultrasound-mediated drug delivery through the blood–brain barrier. *Expert Rev. Neurother.* **2015**, *15*, 477–491. [[CrossRef](#)] [[PubMed](#)]
2. Burgess, A.; Hynynen, K. Microbubble-Assisted Ultrasound for Drug Delivery in the Brain and Central Nervous System. In *Therapeutic Ultrasound; Advances in Experimental Medicine and Biology*; Escoffre, J.-M., Bouakaz, A., Eds.; Springer International Publishing: Cham, Switzerland, 2016; Volume 880, pp. 293–308. ISBN 978-3-319-22535-7.
3. Hynynen, K.; McDannold, N.; Vykhodtseva, N.; Jolesz, F.A. Noninvasive MR Imaging–guided Focal Opening of the Blood-Brain Barrier in Rabbits. *Radiology* **2001**, *220*, 640–646. [[CrossRef](#)] [[PubMed](#)]
4. Marty, B.; Larrat, B.; Van Landeghem, M.; Robic, C.; Robert, P.; Port, M.; Le Bihan, D.; Pernot, M.; Tanter, M.; Lethimonnier, F.; et al. Dynamic Study of Blood–Brain Barrier Closure after its Disruption using Ultrasound: A Quantitative Analysis. *J. Cereb. Blood Flow Metab.* **2012**, *32*, 1948–1958. [[CrossRef](#)] [[PubMed](#)]
5. Conti, A.; Mériaux, S.; Larrat, B. About the Marty model of blood-brain barrier closure after its disruption using focused ultrasound. *Phys. Med. Biol.* **2019**, *64*, 14NT02. [[CrossRef](#)]
6. Downs, M.E.; Buch, A.; Karakatsani, M.E.; Konofagou, E.E.; Ferrera, V.P. Blood-Brain Barrier Opening in Behaving Non-Human Primates via Focused Ultrasound with Systemically Administered Microbubbles. *Sci. Rep.* **2015**, *5*, 15076. [[CrossRef](#)]
7. Downs, M.E.; Buch, A.; Sierra, C.; Karakatsani, M.E.; Chen, S.; Konofagou, E.E.; Ferrera, V.P. Long-Term Safety of Repeated Blood-Brain Barrier Opening via Focused Ultrasound with Microbubbles in Non-Human Primates Performing a Cognitive Task. *PLoS ONE* **2015**, *10*, e0125911. [[CrossRef](#)]
8. FUS Foundation. Available online: <https://www.fusfoundation.org/> (accessed on 1 November 2020).
9. Conti, A.; Magnin, R.; Gerstenmayer, M.; Tsapis, N.; Dumont, E.; Tillement, O.; Lux, F.; Le Bihan, D.; Mériaux, S.; Della Penna, S.; et al. Empirical and Theoretical Characterization of the Diffusion Process of Different Gadolinium-Based Nanoparticles within the Brain Tissue after Ultrasound-Induced Permeabilization of the Blood-Brain Barrier. *Contrast Media Mol. Imaging* **2019**, *2019*, 1–13. [[CrossRef](#)]
10. Mériaux, S.; Conti, A.; Larrat, B. Assessing Diffusion in the Extra-Cellular Space of Brain Tissue by Dynamic MRI Mapping of Contrast Agent Concentrations. *Front. Phys.* **2018**, *6*, 38. [[CrossRef](#)]
11. Valdez, M.A.; Fernandez, E.; Matsunaga, T.; Erickson, R.P.; Trouard, T.P. Distribution and Diffusion of Macromolecule Delivery to the Brain via Focused Ultrasound using Magnetic Resonance and Multispectral Fluorescence Imaging. *Ultrasound Med. Biol.* **2020**, *46*, 122–136. [[CrossRef](#)]
12. Alli, S.; Figueiredo, C.A.; Golbourn, B.; Sabha, N.; Wu, M.Y.; Bondoc, A.; Luck, A.; Coluccia, D.; Maslink, C.; Smith, C.; et al. Brainstem blood brain barrier disruption using focused ultrasound: A demonstration of feasibility and enhanced doxorubicin delivery. *J. Control. Release* **2018**, *281*, 29–41. [[CrossRef](#)]
13. Weber-Adrian, D.; Kofoed, R.H.; Chan, J.W.Y.; Silburt, J.; Noroozian, Z.; Kügler, S.; Hynynen, K.; Aubert, I. Strategy to enhance transgene expression in proximity of amyloid plaques in a mouse model of Alzheimer’s disease. *Theranostics* **2019**, *9*, 8127–8137. [[CrossRef](#)] [[PubMed](#)]
14. Karakatsani, M.E.; Wang, S.; Samiotaki, G.; Kugelman, T.; Olumolade, O.O.; Acosta, C.; Sun, T.; Han, Y.; Kamimura, H.A.S.; Jackson-Lewis, V.; et al. Amelioration of the nigrostriatal pathway facilitated by ultrasound-mediated neurotrophic delivery in early Parkinson’s disease. *J. Control. Release* **2019**, *303*, 289–301. [[CrossRef](#)] [[PubMed](#)]
15. Hsu, Y.-H.; Liu, R.-S.; Lin, W.-L.; Yuh, Y.-S.; Lin, S.-P.; Wong, T.-T. Transcranial pulsed ultrasound facilitates brain uptake of laronidase in enzyme replacement therapy for Mucopolysaccharidosis type I disease. *Orphanet J. Rare Dis.* **2017**, *12*, 109. [[CrossRef](#)] [[PubMed](#)]
16. Mooney, S.J.; Shah, K.; Yeung, S.; Burgess, A.; Aubert, I.; Hynynen, K. Focused Ultrasound-Induced Neurogenesis Requires an Increase in Blood-Brain Barrier Permeability. *PLoS ONE* **2016**, *11*, e0159892. [[CrossRef](#)]

17. Burgess, A.; Dubey, S.; Yeung, S.; Hough, O.; Eterman, N.; Aubert, I.; Hynynen, K. Alzheimer Disease in a Mouse Model: MR Imaging-guided Focused Ultrasound Targeted to the Hippocampus Opens the Blood-Brain Barrier and Improves Pathologic Abnormalities and Behavior. *Radiology* **2014**, *273*, 736–745. [[CrossRef](#)]
18. Lamsam, L.; Johnson, E.; Connolly, I.D.; Wintermark, M.; Hayden Gephart, M. A review of potential applications of MR-guided focused ultrasound for targeting brain tumor therapy. *Neurosurg. Focus* **2018**, *44*, E10. [[CrossRef](#)]
19. Conti, A.; Kamimura, H.A.; Novell, A.; Duggento, A.; Toschi, N. Magnetic Resonance Methods for Focused ultrasound-induced Blood-Brain Barrier Opening. *Front. Phys.* **2020**. [[CrossRef](#)]
20. Kamimura, H.A.; Flament, J.; Valette, J.; Cafarelli, A.; Aron Badin, R.; Hantraye, P.; Larrat, B. Feedback control of microbubble cavitation for ultrasound-mediated blood-brain barrier disruption in non-human primates under magnetic resonance guidance. *J. Cereb. Blood Flow Metab.* **2019**, *39*, 1191–1203. [[CrossRef](#)]
21. Kamimura, H.A.S.; Wang, S.; Wu, S.-Y.; Karakatsani, M.E.; Acosta, C.; Carneiro, A.A.O.; Konofagou, E.E. Chirp- and random-based coded ultrasonic excitation for localized blood-brain barrier opening. *Phys. Med. Biol.* **2015**, *60*, 7695–7712. [[CrossRef](#)]
22. Novell, A.; Kamimura, H.A.S.; Cafarelli, A.; Gerstenmayer, M.; Flament, J.; Valette, J.; Agou, P.; Conti, A.; Selingue, E.; Aron Badin, R.; et al. A new safety index based on intrapulse monitoring of ultra-harmonic cavitation during ultrasound-induced blood-brain barrier opening procedures. *Sci. Rep.* **2020**, *10*, 10088. [[CrossRef](#)]
23. Qin, S.; Caskey, C.F.; Ferrara, K.W. Ultrasound contrast microbubbles in imaging and therapy: Physical principles and engineering. *Phys. Med. Biol.* **2009**, *54*, R27–R57. [[CrossRef](#)]
24. Lentacker, I.; De Cock, I.; Deckers, R.; De Smedt, S.C.; Moonen, C.T.W. Understanding ultrasound induced sonoporation: Definitions and underlying mechanisms. *Adv. Drug Deliv. Rev.* **2014**, *72*, 49–64. [[CrossRef](#)] [[PubMed](#)]
25. Hwang, J.H.; Tu, J.; Brayman, A.A.; Matula, T.J.; Crum, L.A. Correlation between inertial cavitation dose and endothelial cell damage in vivo. *Ultrasound Med. Biol.* **2006**, *32*, 1611–1619. [[CrossRef](#)] [[PubMed](#)]
26. Lee, H.; Kim, H.; Han, H.; Lee, M.; Lee, S.; Yoo, H.; Chang, J.H.; Kim, H. Microbubbles used for contrast enhanced ultrasound and theragnosis: A review of principles to applications. *Biomed. Eng. Lett.* **2017**, *7*, 59–69. [[CrossRef](#)] [[PubMed](#)]
27. Meng, Y.; Pople, C.B.; Lea-Banks, H.; Abrahao, A.; Davidson, B.; Suppiah, S.; Vecchio, L.M.; Samuel, N.; Mahmud, F.; Hynynen, K.; et al. Safety and efficacy of focused ultrasound induced blood-brain barrier opening, an integrative review of animal and human studies. *J. Control. Release* **2019**, *309*, 25–36. [[CrossRef](#)]
28. Kamimura, H.A.S.; Aurup, C.; Bendau, E.V.; Saharkhiz, N.; Kim, M.G.; Konofagou, E.E. Iterative Curve Fitting of the Bioheat Transfer Equation for Thermocouple-Based Temperature Estimation In Vitro and In-Vivo. *IEEE Trans. Ultrason. Ferroelectr. Freq. Control.* **2020**, *67*, 70–80. [[CrossRef](#)]
29. Kooiman, K.; Vos, H.J.; Versluis, M.; de Jong, N. Acoustic behavior of microbubbles and implications for drug delivery. *Adv. Drug Deliv. Rev.* **2014**, *72*, 28–48. [[CrossRef](#)]
30. Delalande, A.; Bastié, C.; Pigeon, L.; Manta, S.; Lebertre, M.; Mignet, N.; Midoux, P.; Pichon, C. Cationic gas-filled microbubbles for ultrasound-based nucleic acids delivery. *Biosci. Rep.* **2017**, *37*, BSR20160619. [[CrossRef](#)]
31. Stride, E.; Segers, T.; Lajoinie, G.; Cherkaoui, S.; Bettinger, T.; Versluis, M.; Borden, M. Microbubble Agents: New Directions. *Ultrasound Med. Biol.* **2020**, *46*, 1326–1343. [[CrossRef](#)]
32. Yildirim, A.; Blum, N.T.; Goodwin, A.P. Colloids, nanoparticles, and materials for imaging, delivery, ablation, and theranostics by focused ultrasound (FUS). *Theranostics* **2019**, *9*, 2572–2594. [[CrossRef](#)]
33. Wu, S.-Y.; Fix, S.M.; Arena, C.B.; Chen, C.C.; Zheng, W.; Olumolade, O.O.; Papadopoulou, V.; Novell, A.; Dayton, P.A.; Konofagou, E.E. Focused ultrasound-facilitated brain drug delivery using optimized nanodroplets: Vaporization efficiency dictates large molecular delivery. *Phys. Med. Biol.* **2018**, *63*, 035002. [[CrossRef](#)] [[PubMed](#)]
34. Fisher, D.G.; Price, R.J. Recent Advances in the Use of Focused Ultrasound for Magnetic Resonance Image-Guided Therapeutic Nanoparticle Delivery to the Central Nervous System. *Front. Pharm.* **2019**, *10*, 1348. [[CrossRef](#)] [[PubMed](#)]
35. Dong, X. Current Strategies for Brain Drug Delivery. *Theranostics* **2018**, *8*, 1481–1493. [[CrossRef](#)] [[PubMed](#)]

36. Shin, J.; Kong, C.; Cho, J.S.; Lee, J.; Koh, C.S.; Yoon, M.-S.; Na, Y.C.; Chang, W.S.; Chang, J.W. Focused ultrasound-mediated noninvasive blood-brain barrier modulation: Preclinical examination of efficacy and safety in various sonication parameters. *Neurosurg. Focus* **2018**, *44*, E15. [[CrossRef](#)]
37. Wu, S.-K.; Chu, P.-C.; Chai, W.-Y.; Kang, S.-T.; Tsai, C.-H.; Fan, C.-H.; Yeh, C.-K.; Liu, H.-L. Characterization of Different Microbubbles in Assisting Focused Ultrasound-Induced Blood-Brain Barrier Opening. *Sci. Rep.* **2017**, *7*, 46689. [[CrossRef](#)]
38. Bing, C.; Hong, Y.; Hernandez, C.; Rich, M.; Cheng, B.; Munaweera, I.; Szczepanski, D.; Xi, Y.; Bolding, M.; Exner, A.; et al. Characterization of different bubble formulations for blood-brain barrier opening using a focused ultrasound system with acoustic feedback control. *Sci. Rep.* **2018**, *8*, 7986. [[CrossRef](#)]
39. Tan, J.-K.Y.; Pham, B.; Zong, Y.; Perez, C.; Maris, D.O.; Hemphill, A.; Miao, C.H.; Matula, T.J.; Mourad, P.D.; Wei, H.; et al. Microbubbles and ultrasound increase intraventricular polyplex gene transfer to the brain. *J. Control. Release* **2016**, *231*, 86–93. [[CrossRef](#)]
40. McDannold, N.; Zhang, Y.; Supko, J.G.; Power, C.; Sun, T.; Peng, C.; Vykhodtseva, N.; Golby, A.J.; Reardon, D.A. Acoustic feedback enables safe and reliable carboplatin delivery across the blood-brain barrier with a clinical focused ultrasound system and improves survival in a rat glioma model. *Theranostics* **2019**, *9*, 6284–6299. [[CrossRef](#)]
41. Yoon, K.; Lee, W.; Chen, E.; Lee, J.E.; Croce, P.; Cammalleri, A.; Foley, L.; Tsao, A.L.; Yoo, S.-S. Localized Blood-Brain Barrier Opening in Ovine Model Using Image-Guided Transcranial Focused Ultrasound. *Ultrasound Med. Biol.* **2019**, *45*, 2391–2404. [[CrossRef](#)]
42. Xhima, K.; Nabbouh, F.; Hynynen, K.; Aubert, I.; Tandon, A. Noninvasive delivery of an  $\alpha$ -synuclein gene silencing vector with magnetic resonance-guided focused ultrasound: Noninvasive Knockdown of Brain  $\alpha$ -Syn. *Mov. Disord.* **2018**, *33*, 1567–1579. [[CrossRef](#)]
43. Arvanitis, C.D.; Askoxylakis, V.; Guo, Y.; Datta, M.; Klopper, J.; Ferraro, G.B.; Bernabeu, M.O.; Fukumura, D.; McDannold, N.; Jain, R.K. Mechanisms of enhanced drug delivery in brain metastases with focused ultrasound-induced blood-tumor barrier disruption. *Proc. Natl. Acad. Sci. USA* **2018**, *115*, E8717–E8726. [[CrossRef](#)] [[PubMed](#)]
44. Pelekanos, M.; Leinenga, G.; Odabae, M.; Odabae, M.; Saifzadeh, S.; Steck, R.; Götz, J. Establishing sheep as an experimental species to validate ultrasound-mediated blood-brain barrier opening for potential therapeutic interventions. *Theranostics* **2018**, *8*, 2583–2602. [[CrossRef](#)] [[PubMed](#)]
45. Park, J.; Aryal, M.; Vykhodtseva, N.; Zhang, Y.-Z.; McDannold, N. Evaluation of permeability, doxorubicin delivery, and drug retention in a rat brain tumor model after ultrasound-induced blood-tumor barrier disruption. *J. Control. Release* **2017**, *250*, 77–85. [[CrossRef](#)] [[PubMed](#)]
46. Alkins, R.; Burgess, A.; Kerbel, R.; Wels, W.S.; Hynynen, K. Early treatment of HER2-amplified brain tumors with targeted NK-92 cells and focused ultrasound improves survival. *Neuro-Oncol.* **2016**, *18*, 974–981. [[CrossRef](#)]
47. Coluccia, D.; Figueiredo, C.A.; Wu, M.Y.; Riemenschneider, A.N.; Diaz, R.; Luck, A.; Smith, C.; Das, S.; Ackerley, C.; O'Reilly, M.; et al. Enhancing glioblastoma treatment using cisplatin-gold-nanoparticle conjugates and targeted delivery with magnetic resonance-guided focused ultrasound. *Nanomed. Nanotechnol. Biol. Med.* **2018**, *14*, 1137–1148. [[CrossRef](#)]
48. Xhima, K.; Markham-Coultes, K.; Nedev, H.; Heinen, S.; Saragovi, H.U.; Hynynen, K.; Aubert, I. Focused ultrasound delivery of a selective TrkA agonist rescues cholinergic function in a mouse model of Alzheimer's disease. *Sci. Adv.* **2020**, *6*, eaax6646. [[CrossRef](#)]
49. Noroozian, Z.; Xhima, K.; Huang, Y.; Kaspar, B.K.; Kügler, S.; Hynynen, K.; Aubert, I. MRI-Guided Focused Ultrasound for Targeted Delivery of rAAV to the Brain. In *Adeno-Associated Virus Vectors*; Castle, M.J., Ed.; Methods in Molecular Biology; Springer New York: New York, NY, USA, 2019; Volume 1950, pp. 177–197. ISBN 978-1-4939-9138-9.
50. Huang, Y.; Alkins, R.; Schwartz, M.L.; Hynynen, K. Opening the Blood-Brain Barrier with MR Imaging-guided Focused Ultrasound: Preclinical Testing on a Trans-Human Skull Porcine Model. *Radiology* **2017**, *282*, 123–130. [[CrossRef](#)]
51. Shin, J.; Kong, C.; Lee, J.; Choi, B.Y.; Sim, J.; Koh, C.S.; Park, M.; Na, Y.C.; Suh, S.W.; Chang, W.S.; et al. Focused ultrasound-induced blood-brain barrier opening improves adult hippocampal neurogenesis and cognitive function in a cholinergic degeneration dementia rat model. *Alzheimers Res.* **2019**, *11*, 110. [[CrossRef](#)]

52. Jung, B.; Huh, H.; Lee, E.; Han, M.; Park, J. An advanced focused ultrasound protocol improves the blood-brain barrier permeability and doxorubicin delivery into the rat brain. *J. Control. Release* **2019**, *315*, 55–64. [[CrossRef](#)]
53. Rich, M.C.; Sherwood, J.; Bartley, A.F.; Whitsitt, Q.A.; Lee, M.; Willoughby, W.R.; Dobrunz, L.E.; Bao, Y.; Lubin, F.D.; Bolding, M. Focused ultrasound blood brain barrier opening mediated delivery of MRI-visible albumin nanoclusters to the rat brain for localized drug delivery with temporal control. *J. Control. Release* **2020**, *324*, 172–180. [[CrossRef](#)]
54. Alecou, T.; Giannakou, M.; Damianou, C. Amyloid  $\beta$  Plaque Reduction With Antibodies Crossing the Blood-Brain Barrier, Which Was Opened in 3 Sessions of Focused Ultrasound in a Rabbit Model: Amyloid  $\beta$  Plaque Reduction With Focused Ultrasound. *J. Ultrasound Med.* **2017**, *36*, 2257–2270. [[CrossRef](#)] [[PubMed](#)]
55. Chu, P.-C.; Chai, W.-Y.; Tsai, C.-H.; Kang, S.-T.; Yeh, C.-K.; Liu, H.-L. Focused Ultrasound-Induced Blood-Brain Barrier Opening: Association with Mechanical Index and Cavitation Index Analyzed by Dynamic Contrast-Enhanced Magnetic-Resonance Imaging. *Sci. Rep.* **2016**, *6*, 33264. [[CrossRef](#)] [[PubMed](#)]
56. Yang, F.-Y.; Chang, W.-Y.; Lin, W.-T.; Hwang, J.-J.; Chien, Y.-C.; Wang, H.-E.; Tsai, M.-L. Focused ultrasound enhanced molecular imaging and gene therapy for multifusion reporter gene in glioma-bearing rat model. *Oncotarget* **2015**, *6*, 36260–36268. [[CrossRef](#)] [[PubMed](#)]
57. Lin, C.-Y.; Hsieh, H.-Y.; Pitt, W.G.; Huang, C.-Y.; Tseng, I.-C.; Yeh, C.-K.; Wei, K.-C.; Liu, H.-L. Focused ultrasound-induced blood-brain barrier opening for non-viral, non-invasive, and targeted gene delivery. *J. Control. Release* **2015**, *212*, 1–9. [[CrossRef](#)] [[PubMed](#)]
58. Horodyckid, C.; Canney, M.; Vignot, A.; Boisgard, R.; Drier, A.; Huberfeld, G.; François, C.; Prigent, A.; Santin, M.D.; Adam, C.; et al. Safe long-term repeated disruption of the blood-brain barrier using an implantable ultrasound device: A multiparametric study in a primate model. *J. Neurosurg.* **2017**, *126*, 1351–1361. [[CrossRef](#)] [[PubMed](#)]
59. Beccaria, K.; Canney, M.; Goldwirt, L.; Fernandez, C.; Piquet, J.; Perier, M.-C.; Lafon, C.; Chapelon, J.-Y.; Carpentier, A. Ultrasound-induced opening of the blood-brain barrier to enhance temozolomide and irinotecan delivery: An experimental study in rabbits. *J. Neurosurg.* **2016**, *124*, 1602–1610. [[CrossRef](#)]
60. Morse, S.V.; Pouliopoulos, A.N.; Chan, T.G.; Copping, M.J.; Lin, J.; Long, N.J.; Choi, J.J. Rapid Short-pulse Ultrasound Delivers Drugs Uniformly across the Murine Blood-Brain Barrier with Negligible Disruption. *Radiology* **2019**, *291*, 459–466. [[CrossRef](#)]
61. Zhang, D.Y.; Dmello, C.; Chen, L.; Arrieta, V.A.; Gonzalez-Buendia, E.; Kane, J.R.; Magnusson, L.P.; Baran, A.; James, C.D.; Horbinski, C.; et al. Ultrasound-mediated Delivery of Paclitaxel for Glioma: A Comparative Study of Distribution, Toxicity, and Efficacy of Albumin-bound Versus Cremophor Formulations. *Clin. Cancer Res.* **2020**, *26*, 477–486. [[CrossRef](#)]
62. Chai, W.-Y.; Chu, P.-C.; Tsai, C.-H.; Lin, C.-Y.; Yang, H.-W.; Lai, H.-Y.; Liu, H.-L. Image-Guided Focused-Ultrasound CNS Molecular Delivery: An Implementation via Dynamic Contrast-Enhanced Magnetic-Resonance Imaging. *Sci. Rep.* **2018**, *8*, 4151. [[CrossRef](#)]
63. Xi, X.-P.; Zong, Y.-J.; Ji, Y.-H.; Wang, B.; Liu, H.-S. Experiment research of focused ultrasound combined with drug and microbubble for treatment of central nervous system leukemia. *Oncotarget* **2018**, *9*, 5424–5434. [[CrossRef](#)]
64. Morse, S.V.; Boltersdorf, T.; Harriss, B.I.; Chan, T.G.; Baxan, N.; Jung, H.S.; Pouliopoulos, A.N.; Choi, J.J.; Long, N.J. Neuron labeling with rhodamine-conjugated Gd-based MRI contrast agents delivered to the brain via focused ultrasound. *Theranostics* **2020**, *10*, 2659–2674. [[CrossRef](#)] [[PubMed](#)]
65. Kung, Y.; Huang, H.-Y.; Liao, W.-H.; Huang, A.P.-H.; Hsiao, M.-Y.; Wu, C.-H.; Liu, H.-L.; Inserra, C.; Chen, W.-S. A Single High-Intensity Shock Wave Pulse With Microbubbles Opens the Blood-Brain Barrier in Rats. *Front. Bioeng. Biotechnol.* **2020**, *8*, 402. [[CrossRef](#)] [[PubMed](#)]
66. Tran, V.L.; Novell, A.; Tournier, N.; Gerstenmayer, M.; Schweitzer-Chaput, A.; Mateos, C.; Jego, B.; Bouleau, A.; Nozach, H.; Winkeler, A.; et al. Impact of blood-brain barrier permeabilization induced by ultrasound associated to microbubbles on the brain delivery and kinetics of cetuximab: An immunopET study using  $^{89}\text{Zr}$ -cetuximab. *J. Control. Release* **2020**, *328*, 304–312. [[CrossRef](#)] [[PubMed](#)]
67. Luo, J.; Xie, C.; Zhang, W.; Cai, Y.; Ding, J.; Wang, Y.; Hao, Y.; Zhang, Y.; Guan, Y. Experimental mouse model of NMOSD produced by facilitated brain delivery of NMO-IgG by microbubble-enhanced low-frequency ultrasound in experimental allergic encephalomyelitis mice. *Mult. Scler. Relat. Disord.* **2020**, *46*, 102473. [[CrossRef](#)]

68. Omata, D.; Maruyama, T.; Unga, J.; Hagiwara, F.; Munakata, L.; Kageyama, S.; Shima, T.; Suzuki, Y.; Maruyama, K.; Suzuki, R. Effects of encapsulated gas on stability of lipid-based microbubbles and ultrasound-triggered drug delivery. *J. Control. Release* **2019**, *311–312*, 65–73. [[CrossRef](#)]
69. Sun, T.; Zhang, Y.; Power, C.; Alexander, P.M.; Sutton, J.T.; Aryal, M.; Vykhodtseva, N.; Miller, E.L.; McDannold, N.J. Closed-loop control of targeted ultrasound drug delivery across the blood–brain/tumor barriers in a rat glioma model. *Proc. Natl. Acad. Sci. USA* **2017**, *114*, E10281–E10290. [[CrossRef](#)]
70. Aryal, M.; Papademetriou, I.; Zhang, Y.-Z.; Power, C.; McDannold, N.; Porter, T. MRI Monitoring and Quantification of Ultrasound-Mediated Delivery of Liposomes Dually Labeled with Gadolinium and Fluorophore through the Blood-Brain Barrier. *Ultrasound Med. Biol.* **2019**, *45*, 1733–1742. [[CrossRef](#)]
71. Yao, X.; Adams, M.S.; Jones, P.D.; Diederich, C.J.; Verkman, A.S. Noninvasive, Targeted Creation of Neuromyelitis Optica Pathology in AQP4-IgG Seropositive Rats by Pulsed Focused Ultrasound. *J. Neuropathol. Exp. Neurol.* **2019**, *78*, 47–56. [[CrossRef](#)]
72. Stavarache, M.A.; Petersen, N.; Jurgens, E.M.; Milstein, E.R.; Rosenfeld, Z.B.; Ballon, D.J.; Kaplitt, M.G. Safe and stable noninvasive focal gene delivery to the mammalian brain following focused ultrasound. *J. Neurosurg.* **2019**, *130*, 989–998. [[CrossRef](#)]
73. Kobus, T.; Zervantonakis, I.K.; Zhang, Y.; McDannold, N.J. Growth inhibition in a brain metastasis model by antibody delivery using focused ultrasound-mediated blood-brain barrier disruption. *J. Control. Release* **2016**, *238*, 281–288. [[CrossRef](#)]
74. Mulik, R.S.; Bing, C.; Ladouceur-Wodzak, M.; Munaweera, I.; Chopra, R.; Corbin, I.R. Localized delivery of low-density lipoprotein docosahexaenoic acid nanoparticles to the rat brain using focused ultrasound. *Biomaterials* **2016**, *83*, 257–268. [[CrossRef](#)] [[PubMed](#)]
75. Song, K.-H.; Fan, A.C.; Hinkle, J.J.; Newman, J.; Borden, M.A.; Harvey, B.K. Microbubble gas volume: A unifying dose parameter in blood-brain barrier opening by focused ultrasound. *Theranostics* **2017**, *7*, 144–152. [[CrossRef](#)] [[PubMed](#)]
76. Hartman, R.K.; Hallam, K.A.; Donnelly, E.M.; Emelianov, S.Y. Photoacoustic imaging of gold nanorods in the brain delivered via microbubble-assisted focused ultrasound: A tool for *in vivo* molecular neuroimaging. *Laser Phys. Lett.* **2019**, *16*, 025603. [[CrossRef](#)] [[PubMed](#)]
77. Papachristodoulou, A.; Signorell, R.D.; Werner, B.; Brambilla, D.; Luciani, P.; Cavusoglu, M.; Grandjean, J.; Silginer, M.; Rudin, M.; Martin, E.; et al. Chemotherapy sensitization of glioblastoma by focused ultrasound-mediated delivery of therapeutic liposomes. *J. Control. Release* **2019**, *295*, 130–139. [[CrossRef](#)]
78. Lin, C.-Y.; Hsieh, H.-Y.; Chen, C.-M.; Wu, S.-R.; Tsai, C.-H.; Huang, C.-Y.; Hua, M.-Y.; Wei, K.-C.; Yeh, C.-K.; Liu, H.-L. Non-invasive, neuron-specific gene therapy by focused ultrasound-induced blood-brain barrier opening in Parkinson’s disease mouse model. *J. Control. Release* **2016**, *235*, 72–81. [[CrossRef](#)]
79. Åslund, A.K.O.; Snipstad, S.; Healey, A.; Kvåle, S.; Torp, S.H.; Sontum, P.C.; de Lange Davies, C.; van Wamel, A. Efficient Enhancement of Blood-Brain Barrier Permeability Using Acoustic Cluster Therapy (ACT). *Theranostics* **2017**, *7*, 23–30. [[CrossRef](#)]
80. Zhang, X.; Hu, J.; Zhao, G.; Huang, N.; Tan, Y.; Pi, L.; Huang, Q.; Wang, F.; Wang, Z.; Wang, Z.; et al. PEGylated PLGA-based phase shift nanodroplets combined with focused ultrasound for blood brain barrier opening in rats. *Oncotarget* **2017**, *8*, 38927–38936. [[CrossRef](#)]
81. Mead, B.P.; Mastorakos, P.; Suk, J.S.; Klibanov, A.L.; Hanes, J.; Price, R.J. Targeted gene transfer to the brain via the delivery of brain-penetrating DNA nanoparticles with focused ultrasound. *J. Control. Release* **2016**, *223*, 109–117. [[CrossRef](#)]
82. Timbie, K.F.; Afzal, U.; Date, A.; Zhang, C.; Song, J.; Wilson Miller, G.; Suk, J.S.; Hanes, J.; Price, R.J. MR image-guided delivery of cisplatin-loaded brain-penetrating nanoparticles to invasive glioma with focused ultrasound. *J. Control. Release* **2017**, *263*, 120–131. [[CrossRef](#)]
83. Curley, C.T.; Mead, B.P.; Negron, K.; Kim, N.; Garrison, W.J.; Miller, G.W.; Kingsmore, K.M.; Thim, E.A.; Song, J.; Munson, J.M.; et al. Augmentation of brain tumor interstitial flow via focused ultrasound promotes brain-penetrating nanoparticle dispersion and transfection. *Sci. Adv.* **2020**, *6*, eaay1344. [[CrossRef](#)]
84. Baghirov, H.; Snipstad, S.; Sulheim, E.; Berg, S.; Hansen, R.; Thorsen, F.; Mørch, Y.; Davies, C.D.L.; Åslund, A.K.O. Ultrasound-mediated delivery and distribution of polymeric nanoparticles in the normal brain parenchyma of a metastatic brain tumour model. *PLoS ONE* **2018**, *13*, e0191102. [[CrossRef](#)] [[PubMed](#)]

85. Åslund, A.K.O.; Berg, S.; Hak, S.; Mørch, Ý.; Torp, S.H.; Sandvig, A.; Widerøe, M.; Hansen, R.; de Lange Davies, C. Nanoparticle delivery to the brain—By focused ultrasound and self-assembled nanoparticle-stabilized microbubbles. *J. Control. Release* **2015**, *220*, 287–294. [[CrossRef](#)] [[PubMed](#)]
86. Liu, Y.; Gong, Y.; Xie, W.; Huang, A.; Yuan, X.; Zhou, H.; Zhu, X.; Chen, X.; Liu, J.; Liu, J.; et al. Microbubbles in combination with focused ultrasound for the delivery of quercetin-modified sulfur nanoparticles through the blood brain barrier into the brain parenchyma and relief of endoplasmic reticulum stress to treat Alzheimer's disease. *Nanoscale* **2020**, *12*, 6498–6511. [[CrossRef](#)] [[PubMed](#)]
87. May, J.-N.; Golombek, S.K.; Baues, M.; Dasgupta, A.; Drude, N.; Rix, A.; Rommel, D.; von Stillfried, S.; Appold, L.; Pola, R.; et al. Multimodal and multiscale optical imaging of nanomedicine delivery across the blood-brain barrier upon sonopermeation. *Theranostics* **2020**, *10*, 1948–1959. [[CrossRef](#)] [[PubMed](#)]
88. Chen, Y.-C.; Chiang, C.-F.; Wu, S.-K.; Chen, L.-F.; Hsieh, W.-Y.; Lin, W.-L. Targeting microbubbles-carrying TGFβ1 inhibitor combined with ultrasound sonication induce BBB/BBB disruption to enhance nanomedicine treatment for brain tumors. *J. Control. Release* **2015**, *211*, 53–62. [[CrossRef](#)]
89. Lin, C.-Y.; Lin, Y.-C.; Huang, C.-Y.; Wu, S.-R.; Chen, C.-M.; Liu, H.-L. Ultrasound-responsive neurotrophic factor-loaded microbubble- liposome complex: Preclinical investigation for Parkinson's disease treatment. *J. Control. Release* **2020**, *321*, 519–528. [[CrossRef](#)]
90. Ha, S.-W.; Hwang, K.; Jin, J.; Cho, A.-S.; Kim, T.Y.; Hwang, S.I.; Lee, H.J.; Kim, C.-Y. Ultrasound-sensitizing nanoparticle complex for overcoming the blood-brain barrier: An effective drug delivery system. *Int. J. Nanomed.* **2019**, *14*, 3743–3752. [[CrossRef](#)]
91. Ilovitsh, T.; Ilovitsh, A.; Foiret, J.; Caskey, C.F.; Kusunose, J.; Fite, B.Z.; Zhang, H.; Mahakian, L.M.; Tam, S.; Butts-Pauly, K.; et al. Enhanced microbubble contrast agent oscillation following 250 kHz insonation. *Sci. Rep.* **2018**, *8*, 16347. [[CrossRef](#)]
92. Wu, S.-Y.; Chen, C.C.; Tung, Y.-S.; Olumolade, O.O.; Konofagou, E.E. Effects of the microbubble shell physicochemical properties on ultrasound-mediated drug delivery to the brain. *J. Control. Release* **2015**, *212*, 30–40. [[CrossRef](#)]
93. Wu, S.-Y.; Aurup, C.; Sanchez, C.S.; Grondin, J.; Zheng, W.; Kamimura, H.; Ferrera, V.P.; Konofagou, E.E. Efficient Blood-Brain Barrier Opening in Primates with Neuronavigation-Guided Ultrasound and Real-Time Acoustic Mapping. *Sci. Rep.* **2018**, *8*, 7978. [[CrossRef](#)]
94. Karakatsani, M.E.; Samiotaki, G.; Downs, M.E.; Ferrera, V.P.; Konofagou, E.E. Targeting Effects on the Volume of the Focused Ultrasound Induced Blood-Brain Barrier Opening in Non-Human Primates in vivo. **2017**, *64*, 798–810. [[PubMed](#)]
95. Samiotaki, G.; Karakatsani, M.E.; Buch, A.; Papadopoulos, S.; Wu, S.Y.; Jambawalikar, S.; Konofagou, E.E. Pharmacokinetic analysis and drug delivery efficiency of the focused ultrasound-induced blood-brain barrier opening in non-human primates. *Magn. Reson. Imaging* **2017**, *37*, 273–281. [[CrossRef](#)] [[PubMed](#)]
96. Sierra, C.; Acosta, C.; Chen, C.; Wu, S.-Y.; Karakatsani, M.E.; Bernal, M.; Konofagou, E.E. Lipid microbubbles as a vehicle for targeted drug delivery using focused ultrasound-induced blood-brain barrier opening. *J. Cereb. Blood Flow Metab.* **2017**, *37*, 1236–1250. [[CrossRef](#)] [[PubMed](#)]
97. Wang, S.; Karakatsani, M.E.; Fung, C.; Sun, T.; Acosta, C.; Konofagou, E. Direct brain infusion can be enhanced with focused ultrasound and microbubbles. *J. Cereb. Blood Flow Metab.* **2017**, *37*, 706–714. [[CrossRef](#)] [[PubMed](#)]
98. Zhang, Y.; Tan, H.; Bertram, E.H.; Aubry, J.-F.; Lopes, M.-B.; Roy, J.; Dumont, E.; Xie, M.; Zuo, Z.; Klivanov, A.L.; et al. Non-Invasive, Focal Disconnection of Brain Circuitry Using Magnetic Resonance-Guided Low-Intensity Focused Ultrasound to Deliver a Neurotoxin. *Ultrasound Med. Biol.* **2016**, *42*, 2261–2269. [[CrossRef](#)] [[PubMed](#)]
99. Karakatsani, M.E.; Kugelman, T.; Ji, R.; Murillo, M.; Wang, S.; Niimi, Y.; Small, S.A.; Duff, K.E.; Konofagou, E.E. Unilateral Focused Ultrasound-Induced Blood-Brain Barrier Opening Reduces Phosphorylated Tau from The rTg4510 Mouse Model. *Theranostics* **2019**, *9*, 5396–5411. [[CrossRef](#)]
100. Yang, Y.; Zhang, X.; Ye, D.; Laforest, R.; Williamson, J.; Liu, Y.; Chen, H. Cavitation dose painting for focused ultrasound-induced blood-brain barrier disruption. *Sci. Rep.* **2019**, *9*, 2840. [[CrossRef](#)]
101. Ye, D.; Sultan, D.; Zhang, X.; Yue, Y.; Heo, G.S.; Kothapalli, S.V.V.N.; Luehmann, H.; Tai, Y.; Rubin, J.B.; Liu, Y.; et al. Focused ultrasound-enabled delivery of radiolabeled nanoclusters to the pons. *J. Control. Release* **2018**, *283*, 143–150. [[CrossRef](#)]

102. Pouliopoulos, A.N.; Jimenez, D.A.; Frank, A.; Robertson, A.; Zhang, L.; Kline-Schoder, A.R.; Bhaskar, V.; Harpale, M.; Caso, E.; Papananou, N.; et al. Temporal Stability of Lipid-Shelled Microbubbles During Acoustically-Mediated Blood-Brain Barrier Opening. *Front. Phys.* **2020**, *8*, 137. [[CrossRef](#)]
103. Galan-Acosta, L.; Sierra, C.; Leppert, A.; Pouliopoulos, A.N.; Kwon, N.; Noel, R.L.; Tambaro, S.; Presto, J.; Nilsson, P.; Konofagou, E.E.; et al. Recombinant BRICHOS chaperone domains delivered to mouse brain parenchyma by focused ultrasound and microbubbles are internalized by hippocampal and cortical neurons. *Mol. Cell. Neurosci.* **2020**, *105*, 103498. [[CrossRef](#)]
104. Chang, E.-L.; Ting, C.-Y.; Hsu, P.-H.; Lin, Y.-C.; Liao, E.-C.; Huang, C.-Y.; Chang, Y.-C.; Chan, H.-L.; Chiang, C.-S.; Liu, H.-L.; et al. Angiogenesis-targeting microbubbles combined with ultrasound-mediated gene therapy in brain tumors. *J. Control. Release* **2017**, *255*, 164–175. [[CrossRef](#)] [[PubMed](#)]
105. Wu, C.-Y.; Fan, C.-H.; Chiu, N.-H.; Ho, Y.-J.; Lin, Y.-C.; Yeh, C.-K. Targeted delivery of engineered auditory sensing protein for ultrasound neuromodulation in the brain. *Theranostics* **2020**, *10*, 3546–3561. [[CrossRef](#)] [[PubMed](#)]
106. Fan, C.-H.; Wang, T.-W.; Hsieh, Y.-K.; Wang, C.-F.; Gao, Z.; Kim, A.; Nagasaki, Y.; Yeh, C.-K. Enhancing Boron Uptake in Brain Glioma by a Boron-Polymer/Microbubble Complex with Focused Ultrasound. *ACS Appl. Mater. Interfaces* **2019**, *11*, 11144–11156. [[CrossRef](#)] [[PubMed](#)]
107. Fan, C.-H.; Chang, E.-L.; Ting, C.-Y.; Lin, Y.-C.; Liao, E.-C.; Huang, C.-Y.; Chang, Y.-C.; Chan, H.-L.; Wei, K.-C.; Yeh, C.-K. Folate-conjugated gene-carrying microbubbles with focused ultrasound for concurrent blood-brain barrier opening and local gene delivery. *Biomaterials* **2016**, *106*, 46–57. [[CrossRef](#)] [[PubMed](#)]
108. Cheng, B.; Bing, C.; Xi, Y.; Shah, B.; Exner, A.A.; Chopra, R. Influence of Nanobubble Concentration on Blood–Brain Barrier Opening Using Focused Ultrasound Under Real-Time Acoustic Feedback Control. *Ultrasound Med. Biol.* **2019**, *45*, 2174–2187. [[CrossRef](#)] [[PubMed](#)]
109. Fan, C.-H.; Cheng, Y.-H.; Ting, C.-Y.; Ho, Y.-J.; Hsu, P.-H.; Liu, H.-L.; Yeh, C.-K. Ultrasound/Magnetic Targeting with SPIO-DOX-Microbubble Complex for Image-Guided Drug Delivery in Brain Tumors. *Theranostics* **2016**, *6*, 1542–1556. [[CrossRef](#)]
110. Zhao, G.; Huang, Q.; Wang, F.; Zhang, X.; Hu, J.; Tan, Y.; Huang, N.; Wang, Z.; Wang, Z.; Cheng, Y. Targeted shRNA-loaded liposome complex combined with focused ultrasound for blood brain barrier disruption and suppressing glioma growth. *Cancer Lett.* **2018**, *418*, 147–158. [[CrossRef](#)]
111. Fan, C.-H.; Ting, C.-Y.; Lin, C.; Chan, H.-L.; Chang, Y.-C.; Chen, Y.-Y.; Liu, H.-L.; Yeh, C.-K. Noninvasive, Targeted and Non-Viral Ultrasound-Mediated GDNF-Plasmid Delivery for Treatment of Parkinson’s Disease. *Sci. Rep.* **2016**, *6*, 19579. [[CrossRef](#)]
112. Long, L.; Cai, X.; Guo, R.; Wang, P.; Wu, L.; Yin, T.; Liao, S.; Lu, Z. Treatment of Parkinson’s disease in rats by Nrf2 transfection using MRI-guided focused ultrasound delivery of nanomicrobubbles. *Biochem. Biophys. Res. Commun.* **2017**, *482*, 75–80. [[CrossRef](#)]
113. Zhao, R.; Jiang, J.; Li, H.; Chen, M.; Liu, R.; Sun, S.; Ma, D.; Liang, X.; Wang, S. Phosphatidylserine-microbubble targeting-activated microglia/macrophage in inflammation combined with ultrasound for breaking through the blood–brain barrier. *J. Neuroinflammation* **2018**, *15*, 334. [[CrossRef](#)]
114. Zhang, N.; Yan, F.; Liang, X.; Wu, M.; Shen, Y.; Chen, M.; Xu, Y.; Zou, G.; Jiang, P.; Tang, C.; et al. Localized delivery of curcumin into brain with polysorbate 80-modified cerasomes by ultrasound-targeted microbubble destruction for improved Parkinson’s disease therapy. *Theranostics* **2018**, *8*, 2264–2277. [[CrossRef](#)] [[PubMed](#)]
115. Pan, M.; Zhang, Y.; Deng, Z.; Yan, F.; Hong, G. Noninvasive and Local Delivery of Adenoviral-Mediated Herpes Simplex Virus Thymidine Kinase to Treat Glioma Through Focused Ultrasound-Induced Blood-Brain Barrier Opening in Rats. *J. Biomed. Nanotechnol.* **2018**, *14*, 2031–2041. [[CrossRef](#)] [[PubMed](#)]
116. Zhao, B.; Chen, Y.; Liu, J.; Zhang, L.; Wang, J.; Yang, Y.; Lv, Q.; Xie, M. Blood-brain barrier disruption induced by diagnostic ultrasound combined with microbubbles in mice. *Oncotarget* **2018**, *9*, 4897–4914. [[CrossRef](#)] [[PubMed](#)]
117. Shen, Y.; Pi, Z.; Yan, F.; Yeh, C.-K.; Zeng, X.; Diao, X.; Hu, Y.; Chen, S.; Chen, X.; Zheng, H. Enhanced delivery of paclitaxel liposomes using focused ultrasound with microbubbles for treating nude mice bearing intracranial glioblastoma xenografts. *Int. J. Nanomed.* **2017**, *12*, 5613–5629. [[CrossRef](#)] [[PubMed](#)]
118. Xu, Y.; Cui, H.; Zhu, Q.; Hua, X.; Xia, H.; Tan, K.; Gao, Y.; Zhao, J.; Liu, Z. Unilateral Opening of Rat Blood-Brain Barrier Assisted by Diagnostic Ultrasound Targeted Microbubbles Destruction. *Biomed. Res. Int.* **2016**, *2016*, 1–10. [[CrossRef](#)] [[PubMed](#)]

119. Shen, Y.; Guo, J.; Chen, G.; Chin, C.T.; Chen, X.; Chen, J.; Wang, F.; Chen, S.; Dan, G. Delivery of Liposomes with Different Sizes to Mice Brain after Sonication by Focused Ultrasound in the Presence of Microbubbles. *Ultrasound Med. Biol.* **2016**, *42*, 1499–1511. [[CrossRef](#)]
120. Cui, H.; Zhu, Q.; Xie, Q.; Liu, Z.; Gao, Y.; He, Y.; Tan, X.; Xu, Y. Low intensity ultrasound targeted microbubble destruction assists MSCs delivery and improves neural function in brain ischaemic rats. *J. Drug Target.* **2020**, *28*, 320–329. [[CrossRef](#)]
121. Blackmore, D.G.; Turpin, F.; Mohamed, A.Z.; Zong, F.; Pandit, R.; Pelekanos, M.; Nasrallah, F.; Sah, P.; Bartlett, P.F.; Götz, J. Multimodal analysis of aged wild-type mice exposed to repeated scanning ultrasound treatments demonstrates long-term safety. *Theranostics* **2018**, *8*, 6233–6247. [[CrossRef](#)]
122. Sun, Y.; Wang, H.; Wang, P.; Zhang, K.; Geng, X.; Liu, Q.; Wang, X. Tumor targeting DVDMS-nanoposomes for an enhanced sonodynamic therapy of gliomas. *Biomater. Sci.* **2019**, *7*, 985–994. [[CrossRef](#)]
123. Pi, Z.; Huang, Y.; Shen, Y.; Zeng, X.; Hu, Y.; Chen, T.; Li, C.; Yu, H.; Chen, S.; Chen, X. Sonodynamic Therapy on Intracranial Glioblastoma Xenografts Using Sinoporphyrin Sodium Delivered by Ultrasound with Microbubbles. *Ann. Biomed. Eng.* **2019**, *47*, 549–562. [[CrossRef](#)]
124. Omata, D.; Hagiwara, F.; Munakata, L.; Shima, T.; Kageyama, S.; Suzuki, Y.; Azuma, T.; Takagi, S.; Seki, K.; Maruyama, K.; et al. Characterization of Brain-Targeted Drug Delivery Enhanced by a Combination of Lipid-Based Microbubbles and Non-Focused Ultrasound. *J. Pharm. Sci.* **2020**, *109*, 2827–2835. [[CrossRef](#)] [[PubMed](#)]
125. Wu, C.-Y.; Huang, R.-Y.; Liao, E.-C.; Lin, Y.-C.; Ho, Y.-J.; Chang, C.-W.; Chan, H.-L.; Huang, Y.-Z.; Hsieh, T.-H.; Fan, C.-H.; et al. A preliminary study of Parkinson's gene therapy via sono-magnetic sensing gene vector for conquering extra/intracellular barriers in mice. *Brain Stimul.* **2020**, *13*, 786–799. [[CrossRef](#)] [[PubMed](#)]
126. Qu, F.; Wang, P.; Zhang, K.; Shi, Y.; Li, Y.; Li, C.; Lu, J.; Liu, Q.; Wang, X. Manipulation of Mitophagy by “All-in-One” nanosensitizer augments sonodynamic glioma therapy. *Autophagy* **2020**, *16*, 1413–1435. [[CrossRef](#)] [[PubMed](#)]
127. Song, K.-H.; Harvey, B.K.; Borden, M.A. State-of-the-art of microbubble-assisted blood-brain barrier disruption. *Theranostics* **2018**, *8*, 4393–4408. [[CrossRef](#)] [[PubMed](#)]
128. Lea-Banks, H.; O'Reilly, M.A.; Hynynen, K. Ultrasound-responsive droplets for therapy: A review. *J. Control. Release* **2019**, *293*, 144–154. [[CrossRef](#)] [[PubMed](#)]
129. Boissenot, T.; Bordat, A.; Fattal, E.; Tsapis, N. Ultrasound-triggered drug delivery for cancer treatment using drug delivery systems: From theoretical considerations to practical applications. *J. Control. Release* **2016**, *241*, 144–163. [[CrossRef](#)] [[PubMed](#)]
130. Sheeran, P.S.; Yoo, K.; Williams, R.; Yin, M.; Foster, F.S.; Burns, P.N. More Than Bubbles: Creating Phase-Shift Droplets from Commercially Available Ultrasound Contrast Agents. *Ultrasound Med. Biol.* **2017**, *43*, 531–540. [[CrossRef](#)]
131. Sheeran, P.S.; Luois, S.H.; Mullin, L.B.; Matsunaga, T.O.; Dayton, P.A. Design of ultrasonically-activatable nanoparticles using low boiling point perfluorocarbons. *Biomaterials* **2012**, *33*, 3262–3269. [[CrossRef](#)]
132. Zhou, Y. Application of acoustic droplet vaporization in ultrasound therapy. *J. Ultrasound* **2015**, *3*, 20. [[CrossRef](#)]
133. Chen, C.C.; Sheeran, P.S.; Wu, S.-Y.; Olumolade, O.O.; Dayton, P.A.; Konofagou, E.E. Targeted drug delivery with focused ultrasound-induced blood-brain barrier opening using acoustically-activated nanodroplets. *J. Control. Release* **2013**, *172*, 795–804. [[CrossRef](#)]
134. Shpak, O.; Verweij, M.; Vos, H.J.; de Jong, N.; Lohse, D.; Versluis, M. Acoustic droplet vaporization is initiated by superharmonic focusing. *Proc. Natl. Acad. Sci. USA* **2014**, *111*, 1697–1702. [[CrossRef](#)] [[PubMed](#)]
135. Ammi, A.Y.; Cleveland, R.O.; Mamou, J.; Wang, G.I.; Bridal, S.L.; O'Brien, W.D. Ultrasonic contrast agent shell rupture detected by inertial cavitation and rebound signals. *IEEE Trans. Ultrason. Ferroelectr. Freq. Control.* **2006**, *53*, 126–136. [[CrossRef](#)] [[PubMed](#)]
136. Borden, M.A.; Song, K.-H. Reverse engineering the ultrasound contrast agent. *Adv. Colloid Interface Sci.* **2018**, *262*, 39–49. [[CrossRef](#)] [[PubMed](#)]
137. Krafft, M.P.; Riess, J.G. Perfluorocarbons: Life sciences and biomedical uses Dedicated to the memory of Professor Guy Ourisson, a true RENAISSANCE man. *J. Polym. Sci. Part. Polym. Chem.* **2007**, *45*, 1185–1198. [[CrossRef](#)]
138. Sheeran, P.S.; Dayton, P.A. Phase-Change Contrast Agents for Imaging and Therapy. *Curr. Pharm. Des.* **2012**, *18*, 2152–2165. [[CrossRef](#)] [[PubMed](#)]

139. Sirsi, S.R.; Borden, M.A. Microbubble compositions, properties and biomedical applications. *Bubble Sci. Eng. Technol.* **2009**, *1*, 3–17. [[CrossRef](#)] [[PubMed](#)]
140. Borden, M.A. Lipid-Coated Nanodrops and Microbubbles. In *Handbook of Ultrasonics and Sonochemistry*; Ashokkumar, M., Ed.; Springer Singapore: Singapore, 2015; pp. 1–26. ISBN 978-981-287-470-2.
141. Sheeran, P.S.; Matsuura, N.; Borden, M.A.; Williams, R.; Matsunaga, T.O.; Burns, P.N.; Dayton, P.A. Methods of Generating Submicrometer Phase-Shift Perfluorocarbon Droplets for Applications in Medical Ultrasonography. *IEEE Trans. Ultrason. Ferroelectr. Freq. Control.* **2017**, *64*, 252–263. [[CrossRef](#)]
142. Sirsi, S.; Feshitan, J.; Kwan, J.; Homma, S.; Borden, M. Effect of Microbubble Size on Fundamental Mode High Frequency Ultrasound Imaging in Mice. *Ultrasound Med. Biol.* **2010**, *36*, 935–948. [[CrossRef](#)]
143. Chomas, J.E.; Dayton, P.; May, D.; Ferrara, K. Threshold of fragmentation for ultrasonic contrast agents. *J. Biomed. Opt.* **2001**, *6*, 141. [[CrossRef](#)]
144. Choi, J.J.; Feshitan, J.A.; Baseri, B.; Wang, S.; Tung, Y.-S.; Borden, M.A.; Konofagou, E.E. Microbubble-Size Dependence of Focused Ultrasound-Induced Blood–Brain Barrier Opening in Mice *In Vivo*. *IEEE Trans. Biomed. Eng.* **2010**, *57*, 145–154. [[CrossRef](#)]
145. Morfin, J.-F.; Beloeil, J.-C.; Tóth, É. Agents de Contraste pour l'IRM. 2014, 23. Available online: <https://www.techniques-ingenieur.fr/base-documentaire/sciences-fondamentales-th8/chimie-organique-et-minerale-42108210/agents-de-contraste-pour-l-irm-af6818/> (accessed on 21 November 2020).
146. Kogan, P.; Gessner, R.C.; Dayton, P.A. Microbubbles in imaging: Applications beyond ultrasound. *Bubble Sci. Eng. Technol.* **2010**, *2*, 3–8. [[CrossRef](#)] [[PubMed](#)]
147. Cheung, J.S.; Chow, A.M.; Guo, H.; Wu, E.X. Microbubbles as a novel contrast agent for brain MRI. *NeuroImage* **2009**, *46*, 658–664. [[CrossRef](#)] [[PubMed](#)]
148. Liao, A.-H.; Liu, H.-L.; Su, C.-H.; Hua, M.-Y.; Yang, H.-W.; Weng, Y.-T.; Hsu, P.-H.; Huang, S.-M.; Wu, S.-Y.; Wang, H.-E.; et al. Paramagnetic perfluorocarbon-filled albumin-(Gd-DTPA) microbubbles for the induction of focused-ultrasound-induced blood–brain barrier opening and concurrent MR and ultrasound imaging. *Phys. Med. Biol.* **2012**, *57*, 2787–2802. [[CrossRef](#)] [[PubMed](#)]
149. Rapoport, N.; Nam, K.-H.; Gupta, R.; Gao, Z.; Mohan, P.; Payne, A.; Todd, N.; Liu, X.; Kim, T.; Shea, J.; et al. Ultrasound-mediated tumor imaging and nanotherapy using drug loaded, block copolymer stabilized perfluorocarbon nanoemulsions. *J. Control. Release* **2011**, *153*, 4–15. [[CrossRef](#)]
150. Timbie, K.F.; Mead, B.P.; Price, R.J. Drug and gene delivery across the blood–brain barrier with focused ultrasound. *J. Control. Release* **2015**, *219*, 61–75. [[CrossRef](#)]
151. Deng, Z.; Sheng, Z.; Yan, F. Ultrasound-Induced Blood-Brain-Barrier Opening Enhances Anticancer Efficacy in the Treatment of Glioblastoma: Current Status and Future Prospects. *J. Oncol.* **2019**, *2019*, 1–9. [[CrossRef](#)]
152. Zaki Ghali, M.G.; Srinivasan, V.M.; Kan, P. Focused Ultrasonography-Mediated Blood-Brain Barrier Disruption in the Enhancement of Delivery of Brain Tumor Therapies. *World Neurosurg.* **2019**, *131*, 65–75. [[CrossRef](#)]
153. Arvanitis, C.D.; Ferraro, G.B.; Jain, R.K. The blood–brain barrier and blood–tumour barrier in brain tumours and metastases. *Nat. Rev. Cancer* **2020**, *20*, 26–41. [[CrossRef](#)]
154. Fontanella, C.; Ongaro, E.; Bolzonello, S.; Guardascione, M.; Fasola, G.; Aprile, G. Clinical advances in the development of novel VEGFR2 inhibitors. *Ann. Transl. Med.* **2014**, *2*, 10.
155. McMahon, D.; Hynynen, K. Acute Inflammatory Response Following Increased Blood-Brain Barrier Permeability Induced by Focused Ultrasound is Dependent on Microbubble Dose. *Theranostics* **2017**, *7*, 3989–4000. [[CrossRef](#)]
156. Carpentier, A.; Canney, M.; Vignot, A.; Reina, V.; Beccaria, K.; Horodyckid, C.; Karachi, C.; Leclercq, D.; Lafon, C.; Chapelon, J.-Y.; et al. Clinical trial of blood-brain barrier disruption by pulsed ultrasound. *Sci. Transl. Med.* **2016**, *8*, 343re2-343re2. [[CrossRef](#)] [[PubMed](#)]
157. Abrahao, A.; Meng, Y.; Llinas, M.; Huang, Y.; Hamani, C.; Mainprize, T.; Aubert, I.; Heyn, C.; Black, S.E.; Hynynen, K.; et al. First-in-human trial of blood–brain barrier opening in amyotrophic lateral sclerosis using MR-guided focused ultrasound. *Nat. Commun.* **2019**, *10*, 4373. [[CrossRef](#)] [[PubMed](#)]
158. Lipsman, N.; Meng, Y.; Bethune, A.J.; Huang, Y.; Lam, B.; Masellis, M.; Herrmann, N.; Heyn, C.; Aubert, I.; Boutet, A.; et al. Blood–brain barrier opening in Alzheimer’s disease using MR-guided focused ultrasound. *Nat. Commun.* **2018**, *9*, 2336. [[CrossRef](#)] [[PubMed](#)]

159. Mainprize, T.; Lipsman, N.; Huang, Y.; Meng, Y.; Bethune, A.; Ironside, S.; Heyn, C.; Alkins, R.; Trudeau, M.; Sahgal, A.; et al. Blood-Brain Barrier Opening in Primary Brain Tumors with Non-invasive MR-Guided Focused Ultrasound: A Clinical Safety and Feasibility Study. *Sci. Rep.* **2019**, *9*, 321. [[CrossRef](#)] [[PubMed](#)]
160. Idbaih, A.; Canney, M.; Belin, L.; Desseaux, C.; Vignot, A.; Bouchoux, G.; Asquier, N.; Law-Ye, B.; Leclercq, D.; Bissery, A.; et al. Safety and Feasibility of Repeated and Transient Blood–Brain Barrier Disruption by Pulsed Ultrasound in Patients with Recurrent Glioblastoma. *Clin. Cancer Res.* **2019**, *25*, 3793–3801. [[CrossRef](#)] [[PubMed](#)]
161. Chen, K.-T.; Lin, Y.-J.; Chai, W.-Y.; Lin, C.-J.; Chen, P.-Y.; Huang, C.-Y.; Kuo, J.S.; Liu, H.-L.; Wei, K.-C. Neuronavigation-guided focused ultrasound (NaviFUS) for transcranial blood-brain barrier opening in recurrent glioblastoma patients: Clinical trial protocol. *Ann. Transl. Med.* **2020**, *8*, 673. [[CrossRef](#)]
162. Maresca, D.; Lakshmanan, A.; Abedi, M.; Bar-Zion, A.; Farhadi, A.; Lu, G.J.; Szablowski, J.O.; Wu, D.; Yoo, S.; Shapiro, M.G. Biomolecular Ultrasound and Sonogenetics. *Annu. Rev. Chem. Biomol. Eng.* **2018**, *9*, 229–252. [[CrossRef](#)]
163. Bourdeau, R.W.; Lee-Gosselin, A.; Lakshmanan, A.; Farhadi, A.; Kumar, S.R.; Nety, S.P.; Shapiro, M.G. Acoustic reporter genes for noninvasive imaging of microorganisms in mammalian hosts. *Nature* **2018**, *553*, 86–90. [[CrossRef](#)]
164. Lakshmanan, A.; Jin, Z.; Nety, S.P.; Sawyer, D.P.; Lee-Gosselin, A.; Malounda, D.; Swift, M.B.; Maresca, D.; Shapiro, M.G. Acoustic biosensors for ultrasound imaging of enzyme activity. *Nat. Chem. Biol.* **2020**, *16*, 988–996. [[CrossRef](#)]

**Publisher’s Note:** MDPI stays neutral with regard to jurisdictional claims in published maps and institutional affiliations.



© 2020 by the authors. Licensee MDPI, Basel, Switzerland. This article is an open access article distributed under the terms and conditions of the Creative Commons Attribution (CC BY) license (<http://creativecommons.org/licenses/by/4.0/>).